

APEX REVIEW • OPEN ACCESS

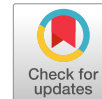
Overview and future perspective of Si tandem solar cells

To cite this article: Masafumi Yamaguchi *et al* 2026 *Appl. Phys. Express* **19** 040105

View the [article online](#) for updates and enhancements.

You may also like

- [A review of recent progress in heterogeneous silicon tandem solar cells](#)
Masafumi Yamaguchi, Kan-Hua Lee, Kenji Araki *et al.*
- [\(Invited\) Perovskite-Based Tandems: Perovskite/Si 2J and Beyond](#)
Jin Young Kim
- [Ultimate efficiency limit of single-junction perovskite and dual-junction perovskite/silicon two-terminal devices](#)
Ibraheem Almansouri, Anita Ho-Baillie and Martin A. Green



Overview and future perspective of Si tandem solar cells

Masafumi Yamaguchi^{1*}, Patrick Schygulla², Ivona Kafedjiska³, Frank Dimroth², and Rutger Schlatmann³

¹Toyota Technological Institute, 2-12-1 Hisakata, Tempaku, Nagoya 468-8511, Japan

²Fraunhofer Institute for Solar Energy Systems, Heidenhofstraße 2, 79110 Freiburg, Germany

³Helmholtz Zentrum Berlin für Materialien und Energie, Schwarzschildstrasse 3, 12489 Berlin, Germany

*E-mail: masafumi@toyota-ti.ac.jp

Received December 16, 2025; revised February 21, 2026; accepted April 1, 2026; published online April 23, 2026

Silicon solar cells are the most established solar cell technology and are expected to dominate the market also in the near future. As state-of-the-art silicon solar cells are approaching the Shockley–Queisser limit (32%–33%), stacking silicon solar cells with other photovoltaic materials to form multi-junction devices is a promising pathway to raise the efficiency. However, many challenges stand in the way of fully realizing the potential of Si tandem solar cells because heterogeneously integrating silicon with other materials often degrades their qualities. Recently, promising efficiencies of 35% and 36.1% have been demonstrated for perovskite/Si 2-junction and III–V/Si 3-junction tandem solar cells, respectively. However, further efficiency improvements and cost reduction of the Si tandem solar cell modules are necessary if they are to compete with Si single-junction solar cell modules. Motivated by the potential, but also by the remaining open questions, this paper presents an overview of recent research endeavors and challenges in the field of Si tandem solar cells. The first part of this review focuses on the integration of silicon with III–V compound semiconductor, perovskites and other materials to form multi-junction solar cells. The second part presents perspectives for Si-based tandem solar cells and modules. Finally, the paper presents an analytical model to compare the material qualities of different types of Si-based tandem solar cells and project the practical efficiency limits, which are found to be more than 39% and 44% for 2-junction and 3-junction Si-based tandem solar cells, respectively. In this paper, cost and reliability issues for Si tandem cells and modules are discussed.

© 2026 The Author(s). Published on behalf of The Japan Society of Applied Physics by IOP Publishing Ltd

1. Introduction

To achieve a sustainable clean energy future, solar photovoltaics (PV) has to contribute in the range of 54–75 TWp by 2050 in several scenarios^{1,2)} requiring significant amounts of high purity crystalline silicon, glass, frames and interconnections. Higher conversion efficiencies can enable a higher resource utilization factor and an even more sustainable energy transition due to a lower CO₂ emission factor per kWh. Si solar cells are by far the most dominant solar cell material in the PV market and are expected to stay dominant in the near future. However, as shown in Fig. 1, the efficiencies of single-junction Si solar cells are approaching their thermodynamic efficiency limit, also known as the Shockley–Queisser limit of 32%–33%.⁴⁾ Figure 1 presents the historical record efficiency of various single-junction solar cells^{3,5,6)} along with their extrapolations,³⁾ mainly bounded by the Shockley–Queisser limit for Si single-junction solar cells.⁴⁾ This analysis was originally presented in Ref. 7. The curves were fitted exclusively by the historical data and assumed that the advances of each technology are largely progressive rather than disruptive. The extrapolations show that the efficiency progress has either already converged or will converge in the near future.

The function chosen in the fitting curves [Eq. (1)] is derived from the diode equation:⁷⁾

$$\eta(t) = \eta_L \{1 - \exp[(a_0 - a)/c]\} \quad (1)$$

where $\eta(t)$ is the time-dependent efficiency, η_L limiting asymptotic maximum efficiency, a_0 is the year for which $\eta(t)$ is zero, a is the calendar year and c is a characteristic development time. Fitting of the curve is done with three parameters which are given in Table I and fitting curves for various single-junction solar cells are shown in Fig. 1. For example, 29% for η_L , 1947.2 for a_0 and 26.8 for c were used

in the case of crystalline Si single-junction solar cells. The function can be fitted relatively well to the past development of best laboratory efficiencies of various solar cells under 1-Sun condition.

An important strategy to boost the efficiency of the solar cells is to stack two or more absorbers with different bandgaps. This so-called ‘multi-junction’ or ‘tandem’ approach⁸⁾ boosts the conversion efficiencies of conventional single-junction solar cells since the high bandgap material on top of the Si absorb high-energy photons that would otherwise be lost via thermalization. The tandem solar cells also reduce non-absorption or below-band-gap losses allowing low-energy photons, which are transmitted by the high-bandgap material, to be absorbed in the underlying low-bandgap material. As Si is a well-established low-bandgap material, most of the novel tandem solar cells explore higher-bandgap top cell materials that could be combined with Si. Perovskites or III–V materials as the upper sub-cells^{9–12)} are expected to reach high efficiency at costs which are acceptable for a high-performance PV module.

Figure 2 shows the chronological efficiency improvement of III–V 3-junction, III–V/Si 3-junction, and perovskite/Si 2-junction tandem solar cells. Dashed lines show the trajectory fitting curve. Table II shows some parameters used for fitting curves. Most recently, 35%¹³⁾ and 36.1%¹⁴⁾ with perovskite/Si 2-junction and III–V/Si 3-junction tandem solar cells have been demonstrated, showing the promise of achieving high-efficiency solar cells via the silicon tandem approach. However, further efficiency improvements and cost reduction for the Si tandem solar cells are necessary in order to reach new markets such as PV-powered electric vehicle (solar-EV) applications¹⁵⁾ for Si tandem solar cells. As shown in Fig. 2 and Table II, the 2-junction and 3-junction Si tandem solar cells are shown to have high-efficiency potential with an efficiency of more than 38% and 43%,



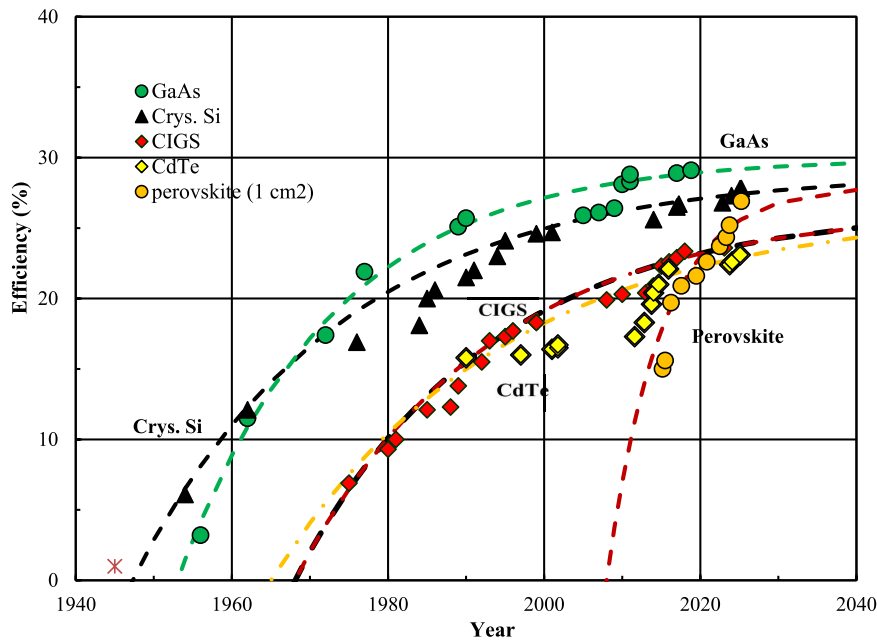


Fig. 1. Chronological efficiency improvement of various single-junction solar cells. Dotted lines show trajectory fitting curves. The fitting procedure is explained in detail and the fitting parameters are listed in Table I. (Adapted with permission from Ref. 3 [Wiley, 2023].)

Table I. Fitting parameters for different single-junction solar cells.

Solar cell	η_L [%]	c [years]	a_0
Single-crystal Si	29	26.8	1947.2
GaAs	30	20	1953
CdTe	26.5	30	1965
CIGS	26.5	25	1968
Perovskite (1 cm ²)	28	7	2008

Table II. Fitting parameters for different multi-junction and Si tandem solar cells.

Solar cell	η_L [%]	c [years]	a_0
III-V 3-junction	43.5	17	1975
III-V/Si 3-junction	43.5	8	2007
Perovskite/Si 2-junction	38.5	7	2010

respectively and are expected to compete with Si single-junction solar cells and to contribute to attainments of the above scenarios.^{1,2)}

Motivated by the progress and future-market potential of Si-based tandem solar cells, this review discusses the latest development of heterogeneous Si tandem solar cells and

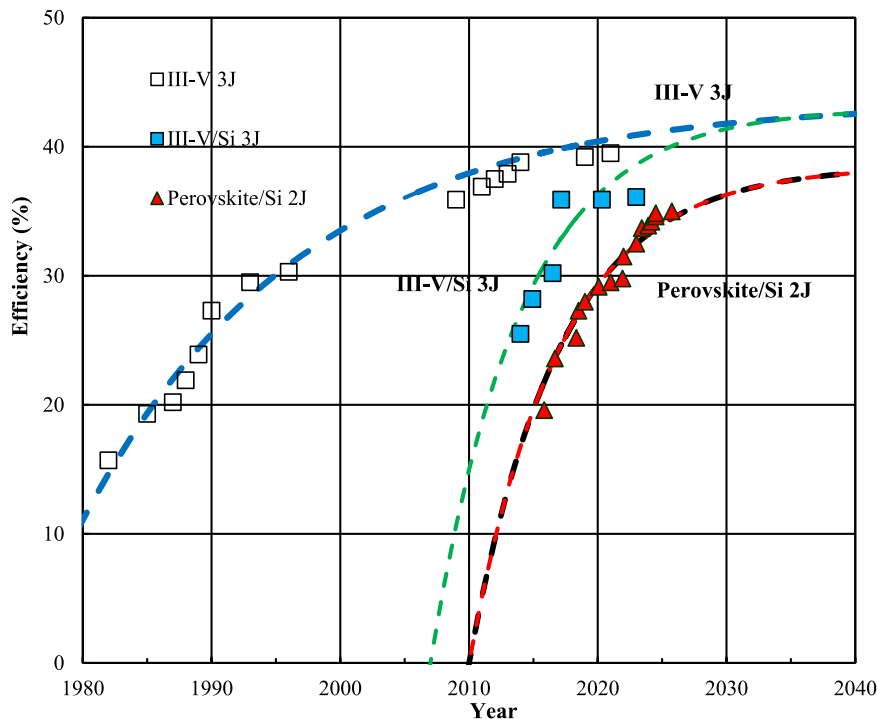


Fig. 2. Chronological efficiency improvement of III-V 3-junction, III-V/Si 3-junction, and perovskite/Si 2-junction tandem solar cells. Dotted lines show trajectory fitting curves.

their tandem perspectives in three core sections. Section 2 presents an overview of three main Si-based tandem technologies (III–V/Si, perovskite/Si, and other Si-based tandem solar cells). Section 3 elaborates on Si-based tandem solar cell modules. Finally, Sect. 4 discusses possible market perspectives of Si-based tandem solar cells, including the main challenges of III–V/Si (Sect. 3.1) and perovskite/Si (Sect. 3.2) tandem solar cells as well as the respective loss, cost analyses and reliability (Sects. 3.3, 3.4 and 3.5, respectively).

2. Overview of Si tandem solar cells

2.1. III–V/Si tandem solar cells

The combination of III–V solar cells with silicon is attractive because III–V materials can be tuned in their absorption characteristics to have optimum bandgap energies in the visible to near infrared spectral range, suitable as top cell materials for 2-junction and 3-junction devices on silicon. The III–V compounds further contribute favorable material properties like direct absorption (which allows to keep the cell layers between 1 and 5 μm thin), high crystalline quality and stability. The latter is an important characteristic of single-crystalline semiconductors which are formed at high temperatures. Due to their superior stability and reliability, III–V cells are used as the power source for today's satellites in space. The major difficulty of bringing the technology to terrestrial applications is cost. Using silicon as the substrate and lowest sub-cell material offers a way to overcome some of the challenges in this context. But it remains a challenge to combine high quality III–V crystals with silicon for reasons like a large difference in lattice constant and thermal expansion coefficient. Furthermore, the interface between silicon and the first III–V layer turns out to be more difficult to control as compared to GaAs on Ge. Therefore, two approaches have been followed: (1) growth of III–V compound solar cells directly on a silicon bottom solar cell and (2) bonding of III–V layers to silicon after release from a GaAs or Ge growth substrate. Both approaches and their main results are discussed in this chapter.

2.1.1. Direct growth of III–V/Si tandem solar cells. Silicon crystals have a lattice constant of 5.431 \AA while the lattice constants of III–V semiconductors with appropriate band gaps for the integration in multi-junction solar cells are significantly higher. As shown in Fig. 3, the band gap of III–V semiconductors tends to decrease with increasing lattice constant. Using detailed-balance assumptions the optimum top cell band gaps for dual- and triple-junction solar cells can be calculated using the software $\text{etaOpt}^{17)}$ and taking literature values for the bowing parameters¹⁸⁾ and Vegard's law the corresponding required lattice constants and compositions of absorber materials follow. For a dual-junction solar cell with an ideal top cell band gap of 1.73 eV the minimum lattice constant amounts to 5.604 \AA for $\text{GaAs}_{0.76}\text{P}_{0.24}$. For a triple-junction solar cell with top and middle cell band gaps of 2.01 eV and 1.50 eV the required minimum lattice constant is even higher with 5.640 \AA . Hence, there is a lattice mismatch of 3.2% in the case of the dual-junction and of 3.8% in the case of a triple-junction that needs to be overcome for monolithic integration on a silicon bottom cell. For a triple-junction device, once the target lattice constant is reached and the middle cell

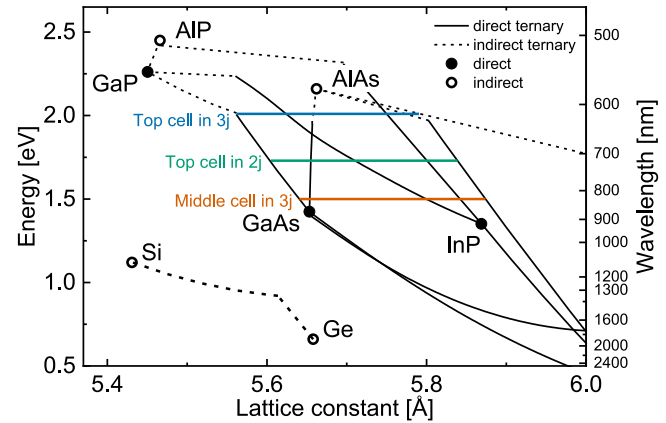


Fig. 3. Band gaps of the most commonly used III–V semiconductors as a function of their lattice constant (adapted from Ref. 16). For a silicon-based multi-junction solar cell the ideal middle and top cell band gaps are indicated by the horizontal lines. Each point on the line corresponds to a certain composition of a ternary (intersection with the black lines) or quaternary III–V semiconductor.

grown, the (Al)GaInP top cell can be grown lattice matched to the middle cell without the need of another buffer layer.

In the 1990s, the first monolithic silicon-based tandem solar cells were demonstrated. Using direct deposition of GaAs or AlGaAs by metalorganic vapor phase epitaxy (MOVPE) on a silicon bottom cell wafer without intermediate buffer layers, the lattice mismatch caused high densities of lattice defects in the III–V top cells. With the help of thermal cycle annealing steps after epitaxial growth, which allowed the atoms to rearrange and thus cured some of the defects, conversion efficiencies of around 20% under the AM0 spectrum were reached.^{19,20)}

Compositionally graded buffer layers have been devised as a promising strategy to mitigate the lattice mismatch.^{21,22)} In such 2–3 μm thick metamorphic buffer structures the lattice constant is gradually increased in successive layers by corresponding changes in the semiconductor composition starting from the lattice constant of silicon. This allows the crystal to release the strain that accumulates during lattice-mismatched growth by forming misfit dislocation defects, irregularities in the crystal lattice with an unoccupied lattice site. Those defects do not impair the device performance as long as they are contained inside the buffer structure and do not penetrate into the absorber layer of the III–V solar cells grown above the structure. At strained interfaces so-called threading dislocations form which propagate vertically along gliding planes. They may become the source of new misfit dislocations in subsequent layers or annihilate with each other or at the crystal boundary. Thus, a finite threading dislocation density (TDD) is present in the electrically active layers after the epitaxial growth of the metamorphic buffer. The minority charge carriers, which are generated in the solar cell upon the absorption of light, can recombine non-radiatively at the threading dislocations since they form energy levels inside the band gap. This results in reduced minority carrier diffusion length L ,²³⁾

$$\frac{1}{L^2} = \frac{1}{L_0^2} + \frac{\pi^3 \text{TDD}}{4}, \quad (2)$$

and in consequence also to a reduced open-circuit voltage. Here, L_0 refers to the diffusion length in the device in the

absence of threading dislocations. The TDD can be determined by counting them on electron channeling contrast images inside a scanning electron microscope setup.²⁴⁾ A point-like signal drop due to enhanced non-radiative recombination can be observed in the vicinity of a threading dislocation. Various strategies have been proposed in the last years to minimize the TDD, for instance by a special design of the metamorphic buffer^{25,26)} or by the introduction of dislocation filtering layers.^{27,28)}

Two promising material systems for the metamorphic buffer layers are $\text{Ga}_x\text{In}_{1-x}\text{As}_y\text{P}_{1-y}$ and $\text{Al}_x\text{Ga}_{1-x}\text{As}_y\text{P}_{1-y}$. As the buffer is positioned between the III–V subcells and the silicon bottom subcell, it is vital to choose a material with a sufficiently high band gap, ideally higher than the one of the lowest III–V absorber layer. Otherwise, parasitic absorption in the buffer structure would result in reduced current generation in the silicon bottom cell. For a dual-junction solar cell $\text{GaAs}_y\text{P}_{1-y}$ is adequate while for a triple-junction solar cell $\text{Al}_x\text{Ga}_{1-x}\text{As}_y\text{P}_{1-y}$ or $\text{Ga}_x\text{In}_{1-x}\text{P}$ are more suitable.²⁹⁾ An alternative buffer material is $\text{Si}_x\text{Ge}_{1-x}$. Due to the indirect nature of its band gap and consequently its weak absorptivity it could be an interesting option despite of its low band gap. Sufficiently thin buffer structures with low parasitic absorption are the prerequisite for SiGe to be successfully used in monolithic III–V/Si multi-junction solar cells.³⁰⁾

Gallium-phosphide (GaP) is the III–V semiconductor with the lowest lattice mismatch to silicon of only 0.36%. Therefore, it is commonly used as the material for nucleation on the silicon wafer surface. Silicon is a covalent crystal, in which the atoms are arranged in the diamond lattice. All atomic bonds are equivalent because all lattice sites are occupied by the same element. In III–V semiconductors, however, the atoms crystallise in the zinc-blende lattice consisting of at least two different elements. Due to the different number of valence electrons of the group-III and the group-V atoms, the stacking must be alternating for all atoms to form covalent bonds. At the interface between the silicon and the III–V crystal, the stacking sequence may be different inside individual growth islands with respect to a global coordinate system when epitaxial growth starts simultaneously on various sites across the crystal. At the border of such anti-phase domains the crystal structure is disturbed leading to another origin of non-radiative recombination. To circumvent this, growth conditions have to be chosen that favour the formation of atomic double-steps on the silicon surface which suppress the occurrence of anti-phase domains.³¹⁾ The GaP nucleation and growth on Si has thus received much attention in the community.³²⁾ To reduce the number of threading dislocations originating at the Si/GaP interface, compressive strained superlattices have been proposed for better control of dislocation evolution.³³⁾

Improvements in the GaP-nucleation and the metamorphic buffer structure have paved the way towards achieving ever higher power conversion efficiencies for monolithic multi-junction solar cells on silicon. The current record efficiency amounts to 23.4% for a $\text{GaAs}_{0.75}\text{P}_{0.25}$ /Si dual-junction^{5,34,35)} and 25.9% for a $\text{Ga}_{0.51}\text{In}_{0.49}\text{P}$ /GaAs/Si triple-junction under the AM1.5G spectrum.^{5,29)} Low values for TDDs reached up to date amount to $3 \times 10^6 \text{ cm}^{-2}$ for a graded buffer from the silicon lattice constant to the one of $\text{GaAs}_{0.76}\text{P}_{0.24}$,³⁴⁾ needed

for a dual-junction solar cell on silicon, and $1.5 \times 10^7 \text{ cm}^{-2}$ for grading further to the GaAs lattice constant.³⁶⁾ A reduction of the dislocation density to around $1 \times 10^6 \text{ cm}^{-2}$ would result in an efficiency improvement to 30% for the III–V/Si-triple-junction solar cell. The fact that the silicon bottom cell serves as a growth substrate for the subsequent deposition of the III–V top structure in a metalorganic or hydride vapour phase epitaxy (HVPE) reactor imposes some constraints on the silicon cell. Flat surfaces of single-crystalline material are required and thus the employed silicon bottom cells must feature a non-textured, crystalline front side to allow for subsequent epitaxial growth.

Another strategy for monolithic integration of III–V top subcells on a silicon bottom cell consists in lateral overgrowth. The silicon wafer is first prestructured by photolithography leaving small apertures from which the III–V layers start to crystallise laterally with potentially low defect density and without anti-phase domains.³⁷⁾ Other innovative approaches to reduce the TDD include aspect ratio trapping,³⁸⁾ nanowire growth,³⁹⁾ or annealing steps.⁴⁰⁾

2.1.2. Bonding of III–V top structures to silicon bottom solar cells. As discussed in the previous paragraph, monolithic growth of III–V semiconductors on silicon wafers results in the formation of dislocation defects which reduce the open-circuit voltage and thus the efficiency of the solar cells. These defects can be reduced to a certain degree by the methods mentioned in the previous paragraph. An alternative approach avoids dislocation defects completely by depositing the III–V top structure lattice-matched separate from the silicon wafer and then combining both structures monolithically by an additional external step. The top and bottom structure can be joined either by a thin amorphous layer as is the case for direct wafer bonding^{41–43)} or by a transparent conductive adhesive as is the case for the gluing approach.^{44–46)} In both cases, the III–V structure is first grown lattice-matched on a III–V substrate, typically GaAs. For a dual-junction on the GaAs lattice constant, the top cell absorber could be made from $\text{Al}_{0.25}\text{Ga}_{0.75}\text{As}$ or $\text{Ga}_{0.65}\text{In}_{0.35}\text{As}_{0.28}\text{P}_{0.72}$, while for a triple-junction the material candidates are $\text{Al}_{0.10}\text{Ga}_{0.41}\text{In}_{0.49}\text{P}$ for the top and $\text{Al}_{0.06}\text{Ga}_{0.94}\text{As}$ or $\text{Ga}_{0.90}\text{In}_{0.10}\text{As}_{0.79}\text{P}_{0.21}$ for the middle cell. The topmost bond layer is highly doped to enable a low series resistance at the connection layer. Furthermore, the epitaxial structure should include a sacrificial layer, typically made from AlAs, at its bottom so that the III–V wafer can be recycled after the solar cell structure is mechanically attached to the silicon wafer.^{47–49)} Such an epitaxial lift-off process is a prerequisite for the bonding approach to become economically viable.

For surface-activated wafer bonding the two wafer surfaces are often first smoothed, for instance by chemical mechanical polishing. Then, inside an evacuated bonding chamber the atomic bonds at the surface are broken by fast ion beams forming a thin amorphous layer. Subsequently, the two wafers are pressed onto each other to join both sides primarily through covalent bonds. The thin amorphous layer connects the two crystals both mechanically and electrically. Wafer bonding requires the wafer surfaces to be planar which again sets a limit to the optical performance of the silicon solar cell. However, the rear-side of the silicon wafer can still be

equipped with an optical structure, e.g. an optical grating, for photocurrent enhancement.^{50,51} The highest efficiency of all silicon-based multi-junction solar cells was obtained by a wafer-bonded $\text{Ga}_{0.51}\text{In}_{0.49}\text{P}/\text{Ga}_{0.91}\text{In}_{0.09}\text{As}_{0.83}\text{P}_{0.17}/\text{Si}$ triple-junction solar cell with 36.1% at the AM1.5G spectrum.¹⁴ Since the amorphous interlayer has a similar refractive index as the surrounding layers, the reflection at this interface is small compared to a tandem cell connected by an adhesive glue. Because of the refractive index mismatch the minimum bond reflectance amounts to around 5% depending on the choice of the adhesive layer in conjunction with the applied ARC.^{52,53} Some groups have also reduced the reflection loss by minimizing the thickness of the bond-layer for example by employing palladium nanoparticle arrays. This resulted in III–V/Si triple-junction solar cells with efficiencies of 30.8% under the AM1.5G spectrum.⁵⁴

So far, we have discussed and implicitly assumed a two-terminal design of the solar cell as employed for single-junction solar cells with merely one contact at the front and one contact on the rear-side of the wafer. Increasing the number of junctions in a solar cell allows to increase the number of terminals as well. Adding two additional electrical contacts, a four-terminal mechanical stack of a III–V top structure with two contacts on top of a silicon bottom cell can be implemented. Alternatively, in a three-terminal device the middle contact can be shared by the III–V and the silicon subcells.⁵⁵ This approach alleviates the constraint of current matching between the subcells, which is required for a series connection of subcells as in a two-terminal configuration. If the solar spectrum and as a consequence the current generation in the different subcells changes over the course of a day then the four-terminal device is less affected in its performance.⁵⁶ Yet, the drawbacks of the three- or four-terminal configuration are a more complex integration of such cells to two-terminal modules⁵⁷ and reflection losses at the refractive index discontinuity. On cell level with size of 1 cm^2 , the highest efficiency achieved for a four-terminal III–V/Si device amounts to 35.9% by a triple-junction and 32.8% by a dual-junction¹⁰ under the AM1.5G spectrum. The fact that the best triple-junction cell efficiency on Silicon has so far been obtained with a two-terminal device rather than a three-terminal cell has no physical reason. But it shows that two-terminal devices can reach similar performance when the subcell currents are well matched. On larger scale, a four-terminal triple-junction module with an area of 775 cm^2 and an efficiency of 33.7% was demonstrated.⁵⁸

2.2. Perovskite/Si tandem solar cells

This section is structured in three sub-sections. First, we discuss the fundamental properties of perovskite solar cells by elaborating on the perovskite crystal structure and underlying material properties; the commonly-used single-junction perovskite solar-cell structures (n-i-p versus p-i-n) and the respective accompanying materials in them [charge-transporting layers and transparent conductive oxides (TCOs)]; and the respective perovskite-based tandem configurations (2-terminal 2T versus 4-terminal 4T). We then proceed to give an overview of the power-conversion efficiency (PCE) development of both 2T and 4T perovskite/Si tandem solar cells in two separate sub-sections. As this section primarily focuses on the rapid development of the performance of perovskite/Si tandem solar cells, their respective

challenges—especially stability and up-scaling—are discussed in more detail in Sect. 4.2.

2.2.1. Fundamentals of perovskite solar cells. Perovskite solar cells were first presented in the research community in 2009 with a modest PCE of around 4%.⁵⁹ By now, their in-lab efficiency has surpassed 26%.⁶⁰ rivaling the performance of market-mature c-Si solar cells and making perovskite solar cells the fastest-ever growing PV technology in terms of their efficiency improvement. Perovskite solar cells display numerous advantageous optoelectronic properties, such as tunability of their direct band gap, high charge-carrier mobility, long bulk lifetimes, large defect tolerance, and (possibly) low-cost and low-temperature fabrication via both solution- and vapour-based deposition techniques. They can also be manufactured either on rigid or on flexible substrates, making them especially attractive for low-weight applications (like flexible and integrated PV) or tandem applications.

Metal-halide perovskites are based on a crystal ABX_3 structure whose bandgap and crystal unit size can be tuned by altering either the X-site^{61,62} or the A-site contribution, respectively.⁶³ For metal-halide perovskite crystals, A and B are mono- and divalent cations, respectively, and X is a halide anion. Most commonly, A is a cation of cesium (Cs^+), methylammonium ($\text{MA} = \text{CH}_3\text{NH}^+$), and formamidinium ($\text{FA} = (\text{NH}_2)_2\text{CH}^+$); B is a lead cation (Pb^{2+}) and X is an iodine and bromide anion (I^- and Br^-). Other A cation can be potassium (K^+), B can be tin (Sn^{2+}) or germanium cations (Ge^{2+}), and X can also be a chlorine (Cl^-) anion.

Perovskite-based tandem solar cells are obtained by combining a wide-bandgap perovskite solar cell ($E_g > 1.65\text{ eV}$) with a low-bandgap solar cell like Si or CIGS, or even with a low-bandgap perovskite solar cell ($E_g \sim 1.1\text{--}1.2\text{ eV}$). The wide-bandgap perovskite is most often the so-called triple-cation ($\text{Cs}_{0.05}(\text{FA}_{0.77}\text{MA}_{0.23})_{0.95}\text{Pb}(\text{I}_{0.77}\text{Br}_{0.23})_3$) or triple-halide perovskite ($\text{Cs}_{0.22}\text{FA}_{0.78}\text{Pb}(\text{I}_{0.85}\text{Br}_{0.15})_3 + 5\% \text{MAPbCl}_3$)⁶⁴ but other absorbers like MAPbI_3 or FAPbI_3 have also been used. Among all perovskite-based tandem solar cells, the perovskite/Si tandem solar cells have been considered the most promising ones for industrialization. The reason is two-fold: on the one hand, Si is a mature, cheap, and abundant PV technology, and the perovskite is seen only as a top-on technology with a negligible additional manufacturing cost. On the other hand, perovskite/Si tandem solar cells—and in particular 2T Si-perovskite tandem solar cells—have demonstrated a significant and quick rise of their in-lab PCEs. With an increasing PCE, one can expect decreasing costs per Wp and decrease in the required installation area—an important aspect for urban and densely-populated areas.

Currently, various companies around the world, such as OxfordPV, Meyer Burger, Enel Green Power (Europe), Tandem PV, Swift Solar, CubicPV (USA), a.o. Microquanta Semiconductor, Renshine Solar, LONGi, Kaneka, Panasonic and Q-Ceslls (Asia), are already working on the up-scaling and market readiness of these solar cells. However, despite an impressive progress in the performance of the perovskite/Si tandem solar cells, they still need to overcome some major challenges—including up-scaling and stability—before they can be sold to customers as PV modules. These challenges are briefly discussed in Sect. 4.

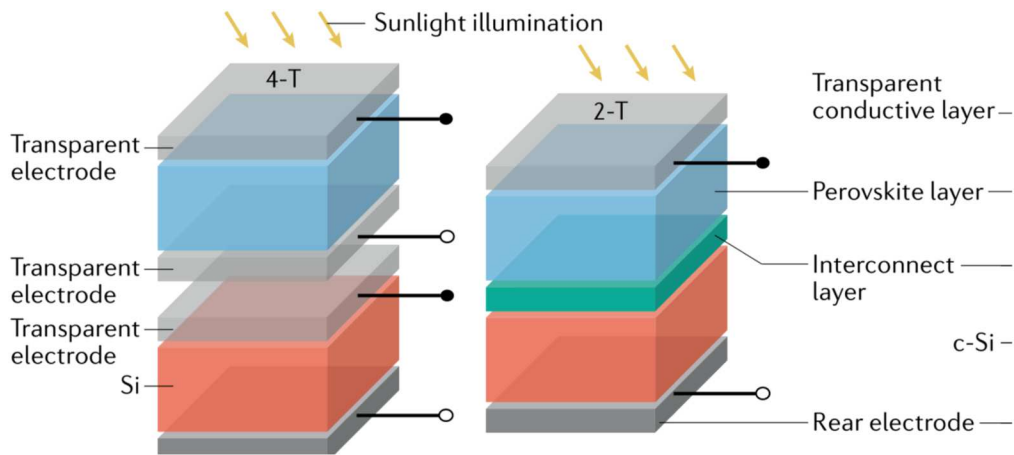


Fig. 4. Simplified visual representation of (a) four-terminal/mechanically-stacked (4 T) tandem with three transparent electrodes and two independent electrical connections versus (b) two-terminal/monolithic (2 T) Si-perovskite tandem solar cell with one transparent electrode and commonly-shared anode and cathode. (Adapted with permission from Ref. 9 [IOP Publishing, 2018].)

A typical perovskite solar cell—regardless if prepared as a single-junction or as a top cell in a tandem solar cell—must always have the following three materials in it: a hole-transporting layer (HTL, p-type material), an electron-transporting layer (ETL, n-type material), and a perovskite absorber (intrinsic (i) material) placed between the ETL and the HTL. The cell is then completed by front and back electrodes which consist of TCOs like indium-doped tin oxide (ITO), indium-doped zinc oxide (IZO), or aluminum-doped zinc oxide; and a metal like silver (Ag) or copper (Cu). The charge-transport layers play a crucial part in the perovskite solar cell as they not only enable an efficient charge separation and a selective charge transport through the device, but also influence the device's open-circuit voltage (V_{oc}), fill factor (FF), and short-circuit current density (J_{sc}). For instance, a poor interface between the perovskite absorber and one or both charge-transporting layers will lead to increased trap-assisted recombination and thus V_{oc} and FF losses.^{65–67} Similarly, poor transparency of the HTL or ETL would lead to parasitic absorption and J_{sc} losses.

Depending on whether the light passes firstly through the HTL or the ETL when the cell is illuminated, perovskite solar cells can be manufactured either in an p-i-n or n-i-p architecture, respectively.

The most commonly used ETL in the p-i-n configuration, and respectively in all highly-efficient perovskite/Si solar cells is C_{60} (buckminsterfullerene). The choice of the HTLs is a bit more complex, as both organic and inorganic materials can be used and they often compete over the points of efficiency and stability.⁶⁸ Organic-based HTLs, such as PTAA, can yield higher efficiencies than some inorganic HTLs, like NiO_x . However, PTAA can be deposited exclusively by spin-coating, which is not attractive for large-scale and industrial applications, and additionally it is characterized by high series resistance and poor wetting.⁶⁹ Other organic HTLs, like self-assembled monolayers (SAMs) based on phosphonic-acid anchoring groups can be deposited by spin-coating, dipping, and even evaporation.⁷⁰ At the moment, these SAMs dominate the research field, and all highly-efficient and world-record perovskite/Si tandem devices are manufactured

with SAMs—either as a stand-alone HTL or in a combination with an inorganic oxide.

In the n-i-p configuration, the most-commonly used ETLs are titanium oxide (TiO_2), zinc oxide (ZnO), and tin oxide (SnO_2). On the HTL side, Spiro-OMeTAD (2,2',7,7'-tetrakis [N,N-di(4-methoxyphenyl)amino]-9-9-spirobifluorene) is still the primary choice; however, Spiro-OMeTAD is very expensive and can be unstable due to the dopants⁷¹ that are used to boost its opto-electronic properties and thus, its performance in the perovskite solar cells.

The perovskite-based tandem solar cells can be manufactured either in a two-terminal (2 T, also known as monolithic) or four-terminal (4 T) configuration (Fig. 4).^{9,72} In the 2 T configuration, the perovskite solar cell is directly deposited on top of the bottom sub-cell and the finished cell (or module, if up-scaled), the two sub-cells are then connected in series and share a common anode and cathode. The monolithic tandem architecture is often considered advantageous over the so-called four-terminal configuration, in which the two sub-cells are mechanically stacked and separately connected, thereby requiring more wiring, packaging, and two extra transparent electrodes compared to the 2 T tandem, subsequently inducing parasitic absorption losses in the tandem. However, the 2 T configuration also limits the processing of the top device as this process should not damage the underlying bottom cell. Additionally, 2 T perovskite tandem solar cells should operate under current matching conditions, meaning that both sub-cells should ideally have an equal J_{sc} (current-matched) or J_{MPP} (power-matched)—a task that has been shown to not be straightforward as each layer in the top device influences how much light is absorbed by both sub-cells. Opposed to the 2 T tandems, the 4 T tandems do not have any processing or current-matching limitations, meaning that the top device can be processed either in an n-i-p architecture (with Spiro-OMeTAD as the HTL and metal oxides as the ETL, both of which require high-temperature processing) or in an p-i-n architecture. For the 2 T configuration, the p-i-n architecture is considered more suitable due to its low-temperature processing not detrimental to the underlying bottom cell as well as due to its longer operating stability compared to the

n-i-p cells under illumination or in outdoor conditions (see stability comparisons in Ref. 73).

In terms of the environmental footprint and economic attractiveness, current studies indicate that 2 T perovskite/Si tandems can be expected to be superior to 4 T perovskite/Si tandems. The production of 2 T Si-perovskite tandem configuration would emit roughly 30% less CO₂ than 4 T Si-perovskite tandems, and it would be additionally cheaper in terms of the manufacturing and balance of system costs due to the usage of less transparent electrodes, wiring, and glass.⁷⁴⁾ Therefore, the 2 T tandem is currently estimated to yield almost twice as cheap LCOE compared to the 4 T tandems, under an assumed PCE of 30% and 30 years lifetime.^{75,76)} However, as perovskites are not yet a state-of-the-art industrialized technology, it is yet open to see if they can deliver both high PCE and operational lifetimes on an industrial-size modules and whether 4 T tandems could potentially become more cost attractive.

2.2.2. Summary of most prominent results of 4 T perovskite/Si tandem solar cells. 4 T Si-perovskite solar cells have demonstrated efficiencies above 22% as early as 2017. This tandem cell used a semi-transparent MAPbI₃ perovskite with Spiro-OMeTAD as the HTL, and it was stacked on top of an interdigitated back contact (IBC) c-Si solar cell. By optimizing the thickness of the sputtered transparent electrode (ITO) and by optimizing the module design, small-area cells (0.13 cm²) and small-area modules (4 cm²) with PCEs as high as 22.6% and 20.2%, respectively were achieved.⁷⁷⁾

In 2020, a rather interesting approach was demonstrated for 4 T Si-perovskite solar cells. The authors increased the optical path length in the perovskite absorber (triple-cation, Cs_{0.05}FA_{0.81}MA_{0.14}PbI_{2.55}Br_{0.45}) by adding a Lewis base in the perovskite precursor solution. This enabled them to increase the perovskite thickness (from 400 to 700 nm), the electron-diffusion length and the J_{sc} in the perovskite, without damaging the morphology of the perovskite films. This perovskite top cell was then combined with two different bottom cells: (1) solution-processed colloidal quantum dot:organic hybrid bottom cell and (2) a bi-facially textured silicon bottom cell. The 4 T Si-perovskite tandem reached a PCE of 28.2%.⁷⁸⁾

In 2021, the mechanical stacking of a semi-transparent perovskite top cell (PCE = 19.8%) to a Si bottom cell (PCE = 8.5%) yielded a 4 T Si-perovskite tandem PCE of 28.3%.⁷⁹⁾ The authors focused on optimizing the transparency and the conductivity of the top electrode for the top cell by using a continuous, ultrathin gold film as the top electrode by introducing a chromium seed layer and varying the thickness of the MgF₂ layer on top. The perovskite absorber was CsI-doped FAPbI₃ and PEAI was used as a surface passivation. The HTL was Spiro-OMeTAD, the ETL was SnO₂. This PCE is the highest-reported PCE for 4 T Si-perovskite solar cells, while simulated results show that a PCE as high as 29.6% should also be achievable.⁸⁰⁾

Some companies and research-industry collaborations are also investing in and potentially aiming at commercialization of 4T-perovskite solar cells. In the Netherlands, Solliance acts as a research-industry alliance and has announced small-sized 29.2%-efficient and 100 cm² 25.6%-efficient 4-T Si-perovskite tandem solar cells in collaboration with TNO.⁸¹⁾

In collaboration with IMEC, a PCE as high as 27.1% on a small-area (0.13 cm²) and 25.3% on a 4 cm² area was obtained with a Si IBC as the bottom cell.⁸²⁾ Microquanta Semiconductor has announced a 26.63%-efficient 4 T Si-perovskite tandem based on PERC with a 20 cm² module area.⁸³⁾ TandemPV in the USA has announced that they have manufactured a 4 T Si-perovskite tandem with an area of 225 cm², but they did not disclose the tandem's PCE.⁸³⁾ CubicPV has announced a PCE >27%, but did not disclose the area of the cell/module.⁸⁴⁾

2.2.3. Summary of most prominent results of 2 T perovskite/Si tandem solar cells. 2 T or monolithic Si-perovskite solar cells are the most investigated and the most efficient tandem configuration. The first reports on these tandem solar cells date to 2015 when efficiencies as high as 18% were demonstrated.⁸⁵⁾ The first certified device was reported in 2017 with an efficiency of 23.6%⁸⁶⁾ and an active area of 0.99 cm². Today, the monolithic Si-perovskite tandem solar cells have demonstrated an 11% efficiency boost compared to the first-certified device and display a certified efficiency of 34.85%⁵⁾ and 35%¹³⁾ on an active area of 1 cm². This section briefly presents the certified world-record devices in a chronological order, which can also be found on the NREL efficiency chart.⁶⁰⁾

The first-certified tandem device in 2017 set the foundation on how tandems are manufactured even nowadays. It was the first demonstration of the tandem-compatible p-i-n single-junction architecture with added ALD-deposited SnO₂ onto the organic C₆₀ n-type contact, protecting the perovskite from sputter damage when sputtering the top TCO (usually IZO). Therefore, since 2017, the tandem solar cell (even when the bottom solar cell is not Si) has been using the following stack: bottom cell—HTL—possible interface modification—perovskite—possible interface modification—C₆₀—SnO₂—ITO or IZO—anti-reflective coating (like LiF)—metal grid.

In 2018, EPFL certified a 25.2%-efficient⁸⁷⁾ Si-perovskite tandem with an active area of 1.42 cm². This publication was the first one to demonstrate that a silicon heterojunction cell with micrometer-sized pyramids of textured monocrystalline silicon can be used as the bottom cell. Previous reports used polished front surface known for higher potential production costs, higher reflection losses and non-ideal light trapping. The authors achieved a conformal coverage of the pyramids by firstly depositing the inorganic part of the perovskite absorber via thermal evaporation and only then spin-coating the organic part. Instead of texturing the bottom cell to improve the light-trapping properties of the tandem, another approach has been to use a textured anti-reflective light management foil. This approach yielded an efficiency as high as 25.5% in 2018.⁸⁸⁾

In the same year, Oxford PV announced and certified firstly a 27.3% and then a 28%-efficient tandem on an active area of 1.09 cm² and 1.03 cm², respectively, but no technical details were revealed for either one of these two cells. Both cells are listed in the NREL record-cell efficiency chart.⁶⁰⁾

The next breakthrough came in 2020 when HZB announced its 29.15%-efficient⁷⁰⁾ tandem solar cell with an active area of 1.06 cm² and Oxford PV its 29.5%-efficient⁶⁰⁾ tandem with an active area of 1.12 cm². The main PCE boost in the device presented by HZB came due to the incorporation of the 2PACz SAM as an HTL and LiF as a passivation

on the perovskite- C_{60} interface.⁷⁰⁾ Starting from 2020, all certified perovskite/Si tandem solar cells use SAMs as HTLs.

In addition to the work on the HTL, in 2020 an incorporation of chlorine (Cl) into the perovskite lattice was introduced as an important advancement for the perovskite absorber, forming a triple-halide alloy of chlorine, bromine and iodine.⁸⁹⁾ The Cl incorporation enabled the bandgap of the top cell to be increased and the photostability to be improved, as demonstrated by the single-junction perovskite device with this absorber that demonstrated a 1000 h stability at 60 °C. The efficiency reached 27%—a significant 2% short of the world-record efficiency—but this study result is of paramount importance for the field since it revealed important insights into the stability of the tandems.

In 2021, HZB announced the next world-record efficiency of 29.8% on an active area of 1.02 cm² (unpublished, but included in Ref. 60). By 2022, EPFL followed with an impressive breakthrough of 31.3%-efficient Si-perovskite monolithic tandem solar cell, demonstrating that the 30% benchmark can be surpassed.⁹⁰⁾ Five months later, HZB followed with its 32.5%-efficient⁹¹⁾ tandem on an active area of 1.01 cm². This publication focused on improving the perovskite- C_{60} interface and substituted LiF with piperazinium iodide as a surface passivation. The perovskite absorber was also altered—instead of using the typical triple cation, the authors used a triple-halide, Cl-containing perovskite absorber ($CS_{0.22}FA_{0.78}Pb(I_{0.85}Br_{0.15})_3 + 5\%$ MAPbCl₃).

By 2023, KAUST has demonstrated firstly a 33.2% and subsequently a 33.7%-efficient Si-perovskite tandem solar cell.⁶⁰⁾ These two results are not yet published, however, the research group has published technical details on a tandem solar cell with a comparable efficiency of 32.5%.⁹²⁾ The main improvement was on the HTL side. As SAMs are only monolayers, reproducible highly-performing tandem solar cells on textured Si bottom cells can be challenging. Therefore, KAUST introduced ultra-thin (5 nm) amorphous IZO as the interconnecting TCO to increase the anchoring density of the SAM. This approach was a follow-up to their idea from 2020 when they have incorporated a thin sputtered NiO_x film to enable the conformal coverage of the pyramids and obtained an efficiency of 25.7%.⁹³⁾ In addition to the IZO layer below the SAM, KAUST also incorporated optical enhancement via equally thin IZO rear electrodes and improved the front contact stacks to eventually demonstrate a 32.5%-efficient solar cell. The 33+% cells are extensions to this work.

Finally, LONGi recently announced their 34.85%⁵⁾ and 35%¹³⁾ certified world-record monolithic Si-perovskite tandem solar cells, which are the highest up-to-date efficiency of monolithic perovskite/Si tandems. Previous to this record, LONGi has announced efficiencies of 33.9% and 34.6% for their perovskite/Si tandem solar cell with an active area of 1 cm² and manufactured on a commercial CZ silicon wafer.⁹⁴⁾ The technical details for both of these devices are not yet revealed.

In addition to LONGi's results, other promising high-efficiency results on industrially-relevant monolithic perovskite/Si tandem solar cells have been demonstrated by Oxford PV, HZB, Q-Cells, and Meyer Burger. OxfordPV has shown 26.9%⁵⁾ on a large area module with an area of 16 023 cm².

Recently, in collaboration with Fraunhofer ISE, they have demonstrated 25% and an output of 421 W^{83,95)} on a module area of 1.68 m². Moreover, they have also announced exports of perovskite/Si modules to the USA. The modules contain 72 cells, a PCE of 24.5%, and can generate up to 20% more energy than conventional single-junction Si modules. Trina has shown 30.6%⁵⁾ on a module with an area of 1185.6 cm². HZB in collaboration with Q-Cells⁹⁶⁾ has demonstrated 28.7% and 29.9%⁹⁷⁾ on a small-scale, but on an industry-feasible and cost-efficient bottom cell structure based on Q-Cells' Q.ANTUM technology. Q-Cells have recently also announced their 28.6% world-record efficiency⁵⁾ for commercially scalable perovskite/Si tandem solar cell on a full-area M10-sized cell. Finally, Meyer Burger has demonstrated a 29.6%-efficient device⁹⁸⁾ with an area of 25 cm².

2.3. Other Si tandem solar cells

Because the ideal bandgap for the top cell material for 2-junction Si tandem solar cells is 1.73 eV,⁹⁾ CdZnTe, MnCdTe and MgCdTe have been studied as II–VI compound top cell materials. 16.8% ($V_{oc} = 1.75$ V, $J_{sc} = 16$ mA cm⁻², FF = 0.6) efficiency with CdZnTe (1.82 eV)/Si 2-junction tandem solar cell has been reported by EPIR Tech.⁹⁹⁾ Current status for Cu₂ZnSnS₄ (1.55 eV)/Si 2-junction tandem solar cell by Tech. Univ. Denmark is 3.9% (Area = 0.146 cm², $V_{oc} = 0.997$ V, $J_{sc} = 8.1$ mA cm⁻², FF = 0.472).¹⁰⁰⁾ The UNIST has reported 17.2% efficiency dye-sensitized (1.76 eV)/Si 2-junction tandem solar cell ($V_{oc} = 1.36$ V, $J_{sc} = 18.3$ mA cm⁻², FF = 0.693).¹⁰¹⁾ The Korea Univ. has reported 15.25% 4-terminal organic (1.73 eV)/Si 2-junction tandem solar cell (Area = 0.08 cm², 4.77%/10.48%, 0.766 V/0.635 V, 10.32 mA cm⁻²/22 mA cm⁻², 0.604/0.75).¹⁰²⁾ Toshiba has demonstrated 24.2% efficiency with Cu₂O (2.1 eV)/Si 2-junction solar cell:¹⁰³⁾ the AIST has reported 12.7% a-Si/nc-Si 2-junction tandem solar cell (Area = 1.000 cm², $V_{oc} = 1.342$ V, $J_{sc} = 13.45$ mA cm⁻², FF = 0.702)⁵⁾ and 14% a-Si/nc-Si/nc-Si 3-junction tandem solar cell (Area = 1.045 cm², $V_{oc} = 1.922$ V, $J_{sc} = 9.94$ mA cm⁻², FF = 0.734).⁵⁾

Figure 5 shows reported efficiencies of various Si tandem solar cells^{5,9–14,99–103)} in comparison with analytical results calculated by using the analytical procedure shown in Sect. 3.3. At present, efficiencies of the Si tandem solar cells by using the other top cell materials are lower compared to III–V/Si and perovskite/Si tandem solar cells. Lower efficiency of Si tandem solar cells composed of the other material top cell is thought to be attributed from lower average external radiative efficiency (ERE) as shown in Fig. 5 that means larger voltage loss due to non-radiative recombination in Si tandem solar cells composed of the other top cell materials compared to III–V/Si and perovskite/Si tandem solar cells.

2.4. Si tandem solar cell modules

Development of high-efficiency solar cell modules is very important for new applications such as VIPV-EV applications.¹⁵⁾ Table III shows the current status of III–V/Si 3-junction and perovskite/Si 2-junction tandem solar cells and modules.^{5,9–14,104)}

Figure 6 shows changes in conversion efficiency of Si, GaAs, CdTe, perovskite single-junction solar cells and modules, and III–V/Si 3-junction and perovskite/Si 2-junction solar cell modules⁵⁾ versus area of solar cells and modules including recent results for 28.6% efficiency⁵⁾

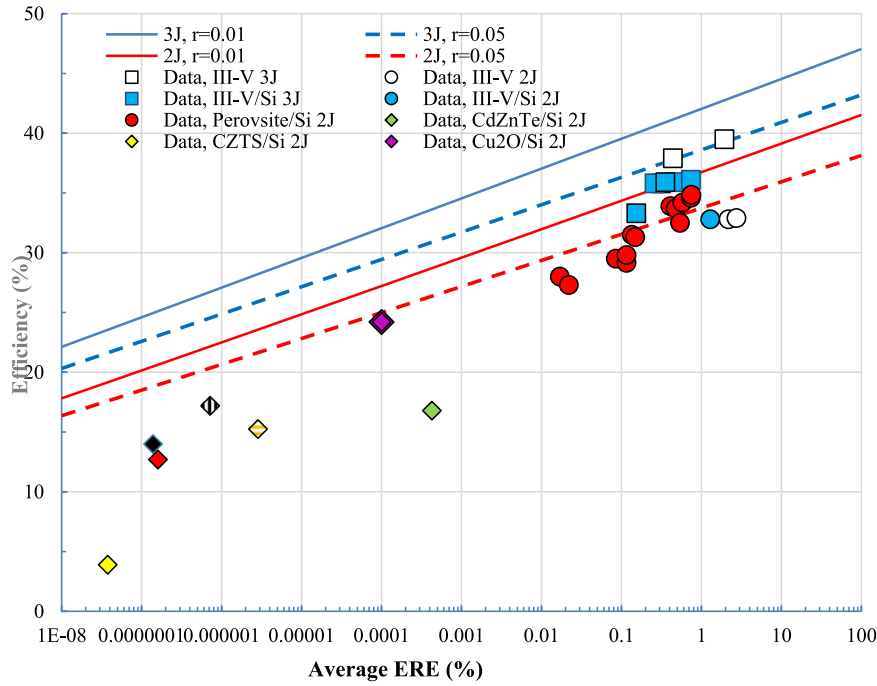


Fig. 5. Reported efficiencies of various Si tandem solar cells^{5,9,99–103} in comparison with results calculated by using analytical procedure shown in Sect. 3.3.

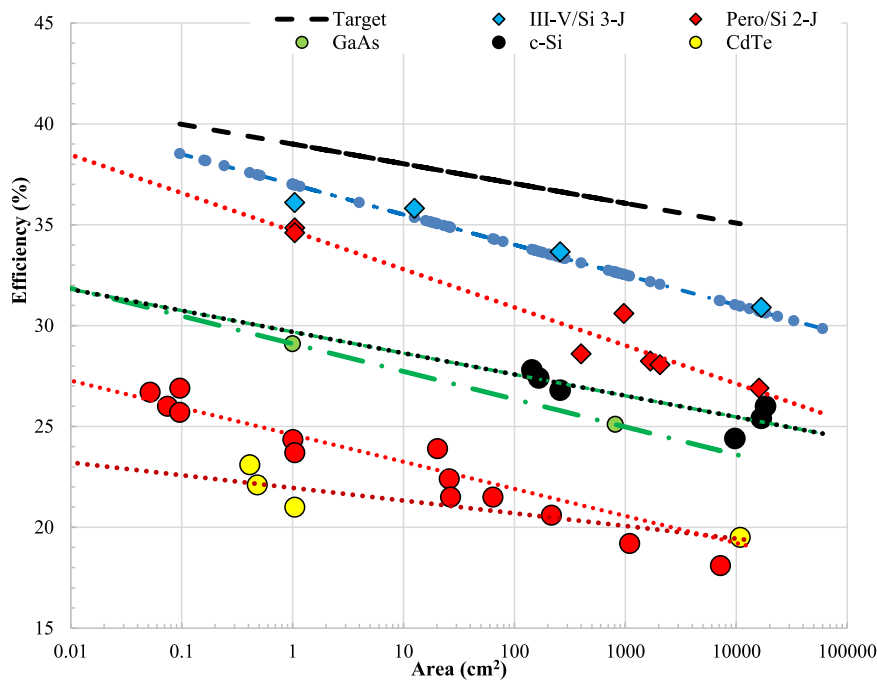


Fig. 6. Changes in conversion efficiency of Si, GaAs, CdTe, perovskite single-junction solar cells and modules, and III–V/Si 3-junction and perovskite/Si 2-junction solar cell modules versus area of solar cells and modules. (Adapted with permission from Ref. 58 [Wiley, 2025].)

Table III. Current status of III–V/Si 3-junction and perovskite/Si 2-junction tandem solar cells and modules.

	Area (cm ²)	Terminal	Efficiency (%)	V _{oc} (V)	J _{sc} (mA cm ⁻²)	FF	Affiliation	Year
III–V/Si 3-J	3.987	2	36.1	3.309	12.7	0.86	FhG-ISE MOLFF	05/2023
	1.002	4	35.9	2.52/0.681	13.6/11	0.875/0.785	NREL,C,S EM, EPFL	02/2017
	775	4	33.7	1.25 V/1.93 V	20.3 A/2.83 A	0.865/0.78	Sharp/Toyota TI	02/2023
Perovskite/Si 2-J	1.0049	2	34.85	1.997	21.08	0.828	Longi	05/2024
	260.9	2	33.0	2.007	19.37	0.848	Longi	04/2025
	1185.6	2	30.6	11.783 V	3.578 A	0.861	Trina	04/2025
	16 023	2	26.9	56.18 V	9.456 A	0.811	Oxford PV	06/2024

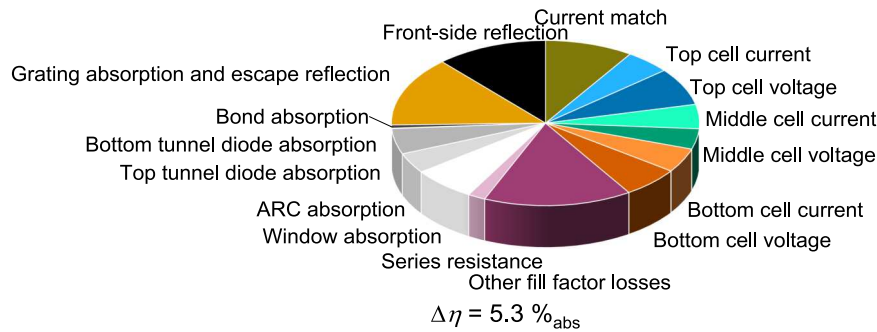


Fig. 7. Loss analysis of the current champion silicon-based triple-junction solar cell compared to the realistic efficiency limit at 41.4%.

perovskite/Si 2-terminal 2-junction solar cell module with an area of 330.56 cm^2 . Our new record efficiency of 33.7% ⁵⁸⁾ for InGaP/GaAs/Si 4-terminal 3-junction tandem solar cell module with an area of 775 cm^2 is also plotted in Fig. 7.

Relative decreasing rates of efficiency with the cell or module area are $-2.4\%/decade$ for III–V/Si 3-junction and $-5.6\%/decade$ for perovskite/Si 2-junction tandem solar cell modules, and $-3.1\%/decade$ for CdTe, $-4.2\%/decade$ for Si, $-5.2\%/decade$ for GaAs, and $-9.8\%/decade$ for perovskite single junction solar cell modules. In order to develop high-efficiency large-area solar cell modules with an efficiency of more than 35%, development of high-efficiency solar cells with an efficiency of more than 39.5% is necessary. It is clear from Fig. 6 that especially, conversion efficiency of perovskite/Si 2-junction tandem and perovskite single-junction solar cells and modules decrease with increase in area of perovskite solar cells and modules. Although the perovskite single-junction solar cell modules are not thought to compete with CdTe solar cell modules, the perovskite/Si tandem solar cell modules are thought to compete with Si single-junction solar cell modules as shown in Fig. 6. Our new world record efficiency (33.7%)⁵⁸⁾ with an area of 775 cm^2 are thought to be due to higher average ERE (0.97%) and FF (0.82) compared to average ERE (0.1%) and FF (0.79) for 28.6% efficiency⁵⁾ perovskite/Si tandem cell module with an area of 330.56 cm^2 . The III–V/Si 3-junction tandem solar cell modules are thought to be very attractive for solar-vehicle applications because of their great potential of longer driving distance of more than 30 km d^{-1} .¹⁵⁾

3. Future perspective of Si tandem solar cells

3.1. III–V/Si

High efficiencies have already been demonstrated for III–V/Si devices. Also, stability and reliability of III–V-based multi-junction solar cells are already widely proven by concentrator PV installations and space satellites. Besides, unless the solar cells are broken, no contamination or toxicity risks are caused by the employment of III–V-containing multi-junction solar cells. Hence, the remaining challenge for the future years is primarily the reduction of cost. As for the epitaxial growth, higher deposition rates will result in lower costs since depreciation and maintenance of the epitaxy machines are among the dominant cost contributions. Using MOVPE, growth rates of $280 \mu\text{m h}^{-1}$ with high precursor incorporation efficiency of 60% have already been demonstrated.^{105,106)} Lower deposition costs can also be achieved by using HVPE. First, in HVPE the precursor

materials are cheaper and second, thanks to its operating conditions close to thermodynamic equilibrium which enables fast reaction kinetics the growth rates are inherently fast with above $300 \mu\text{m h}^{-1}$.¹⁰⁷⁾ Other cheap growth methods such as close-spaced vapour transport, which uses water vapour as carrier agent, are also examined to be used for III–V growth on silicon.¹⁰⁸⁾ A conversion efficiency of 29% for an HVPE-grown four-terminal GaAs/Si solar cell has already been shown.¹⁰⁹⁾

Besides the epitaxy, the cost for solar cell processing needs to be reduced as well for commercial employment. Currently, the state-of-the-art technology for record solar cells requires several expensive materials such as gold and costly steps such as photolithography in a clean room. However, research is ongoing towards replacing these materials and steps, for instance by copper or nickel for inkjet printing and plating¹¹⁰⁾ or screen printing^{111,112)} for the metallisation of the wafer front side.

Apart from cost reduction in the solar cell deposition and processing there is also still potential for efficiency improvements. Combining the best-in-class single-junction results which have already been demonstrated in practice, a realistic upper efficiency limit of 41.4% can be computed.¹¹³⁾ The contributions of various loss channels to the overall difference of the current silicon-based triple-junction champion device performance to this practical limit are presented in Fig. 7. The most readily achievable improvements would be a better current match among the subcells, higher voltages in the top cell, e.g. by increasing the top cell band gap to 2.01 eV, and in the bottom cell, e.g. by passivating the mesa trenches of the solar cells¹¹⁴⁾ or employing larger cell sizes, and reduced parasitic absorption in the AlInP window layer.

In order to assess whether silicon-based multi-junction solar cells are meaningful from a sustainability perspective, a life-cycle analysis was conducted on a monolithic III–V/Si dual-junction solar cell. It found that given the right choices of materials and techniques for deposition and processing, the higher environmental impact of the additional steps can be compensated by the superior efficiency compared to a silicon single-junction solar cell.¹¹⁵⁾ Both the bonding approach and the direct growth using a metamorphic buffer have a climate impact associated with them that is smaller by around a quarter in comparison to a silicon single-junction solar cell. Also, the ecological risk of releasing III–V compound semiconductors into the environment over the cell lifetime in outdoor operation was found to be negligible.¹¹⁶⁾

3.2. Perovskite/Si

As highly-efficient perovskite/Si tandem solar cells have consistently been demonstrated across varying research groups, the research focus by now has shifted towards three core pillars: reproducible fabrication of (1) stable, (2) large-area and, to a lesser extent, (3) low-toxicity perovskite/Si tandem solar cells.

The instability of the perovskite solar cells (regardless if single or tandem) is the most pressing issue since the high PCE of the tandems will not be of much relevance if the devices cannot survive long-term field operation. The perovskite absorber, the defects in the absorber, at the grain boundaries or at the interfaces, the metal electrodes, and the charge-transport layers all affect the cells' stability.⁸³⁾ Some of the most prominent strategies that have been used to stabilize the tandems include, but are not limited to, using more stable HTLs such as SAMs and NiO_x,⁹³⁾ incorporating Cl into the perovskite lattice to suppress a possible Br segregation into the wide-bandgap perovskite,⁹¹⁾ and interface and grain-boundary passivation to suppress the trap density, trap-assisted recombination, and possible ion migration⁶⁶⁾—all of which can severely hinder the cells' stability. The ion migration has also been tackled by exploring perovskite precursor solution with Br or I excess, such that upon (possible) migration of these elements, the perovskite crystal would still remain unaffected.^{117,118)}

However, the stability is not only a matter of solar-cell fabrication but also of stability testing. Faced with a plethora of stability tests, the perovskite-based solar cells can often pass one, but fail another stability test, making their one-on-one comparison and long-term outdoor performance forecasting challenging.^{83,119)} On the one hand, truly long-term (of at least several months) stability tests under outdoor conditions are scarce,^{120,121)} though rising, with several reports from Germany (for single-junction perovskite solar cells¹¹⁹⁾ and Saudi Arabia. On the other hand, accelerated-aging tests performed under a controlled environment and for specific stressors (for instance, damp-heat, light cycling, MPP tracking at room or elevated temperatures etc.) can and should be used to model the long-term performance of devices.⁸³⁾ However, despite numerous accelerated aging tests across varying laboratories around the world, there is still no consensus regarding the expected lifetime of today's state-of-the-art perovskite/Si tandem solar cells, as some predict lifetimes as low as 3–5 years, and others predict lifetimes above 15 years as shown in Sect. 3.5.

The large uncertainty in the stability of the devices means that the LCOE of the tandems should be re-evaluated as a function of both the annual degradation rate (ADR) and the PCE of the cells. For an assumed 2 T perovskite/Si tandem efficiency of 30%, the LCOE modeling has shown that the LCOE breaks even up to a 1.5% ADR, while a 2% ADR (module lifetime reduction of around 10 years) would remove the tandem's LCOE benefit over the single-junction Si module. If the tandems can be more stable, then the PCE can be lowered; or, the other way around—if the module PCE is lower than 30%, then the tandems would need to be significantly more stable than 10 years.⁷⁶⁾

In addition to the stability issue, the so-called “up-scaling gap” results only in a limited number of published large-area tandems with large efficiencies. The up-scaling is by nature a

question of demonstrating and then reproducibly delivering a high PCE on a module area at minimal cost; at one level deeper, it is a question of how to fine-tune the deposition processes of all layers in the device to obtain high-quality films and interfaces with low recombination velocities and trap densities. Therefore, the PCE gap between the small-scale cells and the larger-area modules primarily originates in the difference in quality, uniformity, or morphology of the perovskite film made by methods different than spin-coating (used in all small-scale record devices), such as co-evaporation, slot-die or blade coating, or ink-jet printing.¹²²⁾

Concluding which fabrication method has the best commercialization potential is also not straight-forward, as this answer depends on the complex interplay between cost, performance, and process fine-tuning. For instance, vapour-based fabrication methods, such as co-evaporation, eliminate the need to use toxic solvents, but due to the high-vacuum environment they are more expensive and slower than solution-based deposition techniques such as slot-die or blade coating. Inkjet printing, for instance, has not yielded a very high PCE on large-area single-junction (record ink-jet single-junction perovskite solar cell has a PCE of 21%,¹²³⁾ but an area of only 0.1 cm² or tandem devices in the research community. However, it has enabled Panasonic to manufacture their commercially relevant single-junction perovskite modules¹²⁴⁾ with an area of 802 cm², showing that in principle, ink-jet printing could be also a viable deposition technique when manufacturing perovskite/Si tandems as well. This discrepancy between the research- and industry-based results shows that one fabrication method is not per se intrinsically good or bad, and that the key factor is the optimization of the ink and deposition parameters.

Finally, perovskite/Si tandem solar cells face a toxicity issue due to the usage of toxic solvents in the solution-based processing of the perovskite solar cell and the presence of Pb in the perovskite absorber. By now there is a common agreement that the most-commonly used dimethylformamide (DMF) solvent needs to be substituted with greener solvents like dimethyl sulfoxide, acetonitrile, ethyl acetate, or anisole. However, as the solvents play a crucial role into the ink formation and its properties, the toxic-solvents substitution is not just a question of toxicity, but also of scalability.¹²⁵⁾ To be more precise, the high performance of the solution-based scalable coating or printing deposition techniques is primarily predetermined by the ink's physical and chemical properties. Therefore, it is yet an open question how the DMF-free inks will impact the perovskite-absorber morphology and the device's interfaces at a large scale. If opting for vapour-based deposition techniques, this issue is eliminated from the start.

Regarding the Pb-toxicity issue, the scientific community has diverged on the opinion whether we should improve the performance of Pb-free,¹²⁶⁾ Sn-based perovskite compositions,¹¹⁸⁾ or work on either Pb-immobilization¹²⁷⁾ or Pb-capture¹²⁸⁾ approaches. However, as Sn-based perovskite solar cells are severely limited in their efficiency and stability,¹²⁵⁾ and they have not yet been demonstrated to work as a high-bandgap sub-cell in perovskite/Si tandem solar cells, all prominent research and industrial endeavors focus on Pb-based solar cells. Therefore, the research focus has also shifted towards the investigation of Pb-capture

approaches either via the usage of materials that react with Pb (chemical-based capture) or via the usage of sturdy encapsulation (mechanical prevention of Pb leakage), as well as evaluating the possible risk of Pb leakage into the environment.

3.3. Loss analysis of Si tandem solar cells

In this section, loss elements for the various Si tandem solar cells are discussed in comparison with those of single-junction, III–V 2-junction and 3-junction solar cells.

Non-radiative recombination loss of solar cells is estimated from voltage loss of solar cells.

Open-circuit voltage is expressed by.¹²⁹⁾

$$V_{oc} = V_{oc,rad} + (kT/q) \ln(ERE), \quad (3)$$

where the second term shows non-radiative voltage loss, and $V_{oc,rad}$ is radiative open-circuit voltage and is given by¹²⁹⁾

$$V_{oc,rad} = (kT/q) \ln(JL(V_{oc,rad})/J_{0,rad+1}), \quad (4)$$

where $JL(V_{oc,rad})$ is photo-current at open-circuit in the case of only radiative recombination and $J_{0,rad}$ is saturation current density in the case of only radiative recombination. $\Delta V_{oc,rad} = E_g/q - V_{oc,rad}$ value of 0.26 V^{130–132)} for Si, and in the Sects. 3 and 4, 0.29 V for InGaP, 0.274 V for GaAs, 0.26 V for InGaAs and 0.28 V for perovskite^{130–132)} were used.

In the case of multi-junction tandem solar cells, we defined average ERE (EREave) by using average V_{oc} loss.¹³³⁾

$$\sum(V_{oc,n} - V_{oc,rad,n})/n = (kT/q) \ln(EREave), \quad (5)$$

where n is the number of junctions.

FF is dependent upon V_{oc} and ideal FF FF_0 used in the calculation is empirically expressed by,¹³⁴⁾

$$FF_0 = [V_{oc} - \ln(V_{oc} + 0.72)] / (V_{oc} + 1), \quad (6)$$

where V_{oc} is normalized open-circuit voltage and is given by

$$V_{oc} = V_{oc}/(nkT/q). \quad (7)$$

The FF is decreased as the series resistance R_S increases and the shunt resistance decreases.

The shunt resistance R_{Sh} of a solar cell is approximated by

$$FF \approx FF_0(1 - r_s)(1 - 1/r_{sh}) \approx FF_0(1 - r_s - 1/r_{sh}). \quad (8)$$

The characteristic resistance R_{CH} is expressed by¹³⁴⁾

$$R_{CH} = V_{oc}/I_{sc}. \quad (9)$$

In the calculation, highest values obtained experimentally were used as J_{sc} . V_{oc} and FF were calculated by Eqs. (3)–(9) and conversion efficiency potential of various solar cells were calculated as a function of ERE or average ERE.

Practical limiting efficiencies of various solar cells were estimated by assuming ERE or average ERE of 10%, optical loss of 3% and resistance loss of 2%. In the case of GaAs single-junction solar cells an ERE of 50% was used because higher ERE values of more than 30% were realized for GaAs solar cells.¹³⁵⁾ The recombination loss was estimated by using V_{oc} values and Eqs. (3)–(5), the optical loss was estimated by using J_{sc} values determined from photon flux as a function of bandgap energy, and resistance loss was estimated by using FF and Eqs. (6)–(9).

Figure 8 shows analytical results for non-radiative recombination, optical and resistance losses of Si tandem solar cells in comparison with those of single-junction and III–V 3-junction and 2-junction solar cells. The 2-junction and 3-junction Si tandem solar cells have higher potential efficiency of 39.1% and 44.5%, respectively. Those efficiencies show good agreement with practically limiting efficiencies of 38.5% and 43.5% shown in Fig. 2 and Table II. For 36.1%¹⁴⁾ III–V/Si 3-junction cells, there are still 8.4% efficiency improvement potential with 3.5%, 4.1% and 0.8% by reduction in recombination loss, optical loss and resistance loss, respectively. For 34.85%⁵⁾ perovskite/Si 2-junction cells, there are still 4.25% efficiency improvement potential with 2.5%, 0.65% and 1.1% by reduction in recombination loss, optical loss and resistance loss, respectively. Because 3-junction solar cells have higher potential efficiency of more than 44.5%, development of high-efficiency perovskite based 3-junction solar cells is very attractive as well as III–V/Si 3-junction solar cells.

3.4. Cost analysis of Si tandem solar cells

In this section, cost analytical results for the Si tandem solar cell modules are compared with trends in Si and CdTe single-junction solar cell modules.

Figure 9 shows cost analytical results for III–V/Si^{10,136)} and perovskite/Si¹³⁷⁾ tandem solar cell modules in comparison with module price and cost trends in Si¹³⁸⁾ and CdTe¹³⁹⁾ single-junction solar cell modules and cost analytical results for perovskite single-junction cell modules.¹⁴⁰⁾ Cost analytical results for III–V/Si and perovskite/Si tandem solar cells show the similar cost trends in CdTe single-junction solar cell modules. However, cost reduction of Si tandem solar cell modules by technology development and increasing market volume with a cumulative module production volume of more than 10 GW is necessary in order to realize cost targets of the Si tandem solar cell modules to come with current price of Si and CdTe solar cell modules.

3.5. Reliability issues of Si tandem solar cells

Although the perovskite and perovskite tandem solar cells are expected as next generation solar cell modules, their reliability is one of the big problems to be solved^{141–143)} as presented in sub-section in 3.2. On the other hands, Si¹⁴⁴⁾ and III–V compound^{145,146)} space solar cells have been tested under accelerating test condition over 150 °C and demonstrated to be reliable as shown in Fig. 10. Thermal degradation rates for perovskite, perovskite/Si tandem, Si and III–V compound solar cells are approximated by the following equations:

$$\begin{aligned} \text{TDR}[1/h](\text{perovskite by NREL})^{144)} \\ = 27640 * \text{EXP}(-0.58 \text{ eV}/kT), \end{aligned} \quad (10)$$

$$\begin{aligned} \text{TDR}[1/h](\text{perovskite by Sekisui})^{145)} \\ = 25668 * \text{EXP}(-0.61 \text{ eV}/kT), \end{aligned} \quad (11)$$

$$\text{TDR}[1/h](\text{Si}^{147)}) = 2.2248 * \text{EXP}(-0.43 \text{ eV}/kT), \quad (12)$$

$$\begin{aligned} \text{TDR}[1/h](\text{III - V 3 J and GaAs})^{148,149)} \\ = 0.2192 * \text{EXP}(-0.38 \text{ eV}/kT). \end{aligned} \quad (13)$$

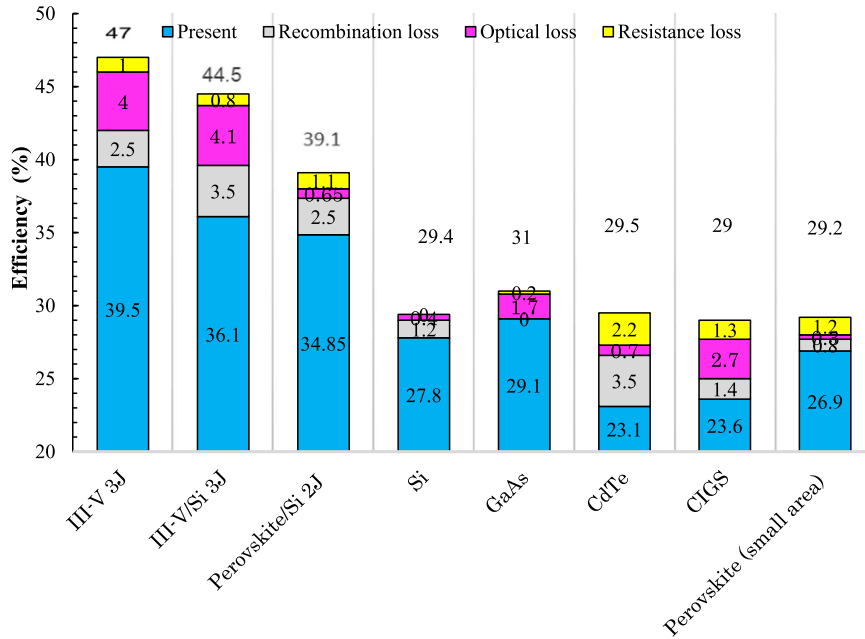


Fig. 8. Analytical results for non-radiative recombination, optical and resistance losses of Si tandem solar cells in comparison with those of single-junction and III-V 3-junction and 2-junction solar cells. (Adapted with permission from Ref. 58 [Wiley, 2025].)

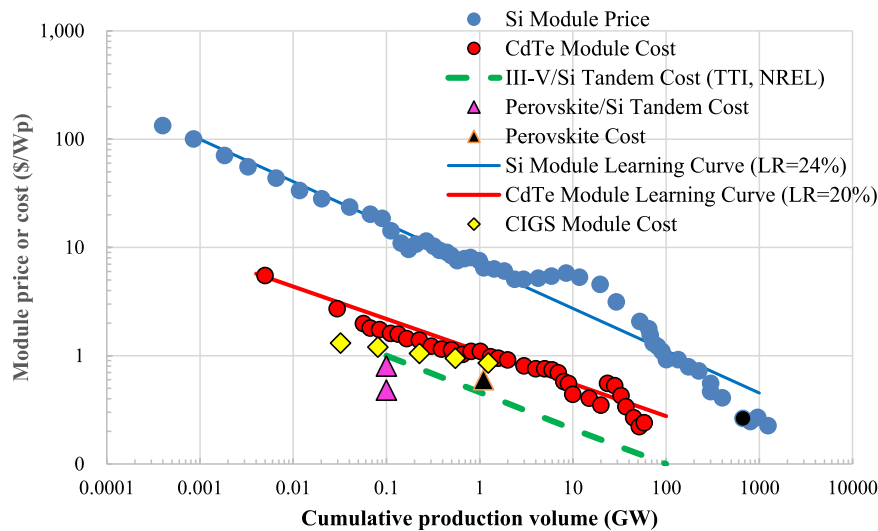


Fig. 9. Cost analytical results for III-V/Si and perovskite/Si tandem solar cell modules in comparison with module price and cost trends in Si and CdTe single-junction solar cell modules and cost analytical results for perovskite single-junction solar cell modules.

Where h is the hour, k is the Boltzmann constant and T is the absolute temperature.

Temperature rise of solar cell modules in major cities in the world was estimated by using our previous paper.¹⁴⁷⁾ Total temperature rise ΔT_T of solar cell modules by considering effects of ambient temperature T_0 is given by

$$\begin{aligned} \Delta T_T = T_m - T_0 = & 0.1844 * T_0 [^\circ\text{C}] + c * e^{(d * v)} \\ & + G * e^{(a+b * v)} = 0.1844 * T_0 \\ & - 9 * e^{(-0.16v)} + G * e^{(-2.7-0.17v)}, \end{aligned} \quad (14)$$

where T_m is the module temperature [$^\circ\text{C}$], T_0 is the ambient temperature [$^\circ\text{C}$], G is the solar irradiation incident on the module surface [W m^{-2}], and v is the wind speed [m s^{-1}]. a , b , c and d are the empirically-determined coefficients. In this study, empirically-determined coefficients a , b , c , and d determined are -2.7 , -0.17 , -9 , and -0.16 , respectively.

By using the average solar irradiance [kW m^{-2}] and average wind speed [m s^{-1}] taken from the references¹⁴⁸⁾ in Glasgow, Tokyo and Phoenix, the temperature rise of solar cell modules was calculated by using Eq. (14). Outdoor degradation of perovskite/Si tandem solar cells was estimated by combining thermal degradation of perovskite and Si solar cells and using Eqs. (11) and (12). In the similar way, outdoor degradation of III-V/Si tandem solar cells was estimated by combining thermal degradation of III-V and Si solar cells and using Eqs. (13) and (12).

Figure 11 shows analytical results for outdoor degradation of perovskite/Si and III-V/Si tandem solar cells to be operated in Phoenix, Tokyo and Glasgow. At present, reliability of perovskite/Si tandem solar cells is poor as the time to reach 80% of initial efficiency estimated for perovskite/Si tandem solar cells operating in Phoenix, Tokyo and Glasgow is 2.7 years, 6.7 years and 24.3 years,

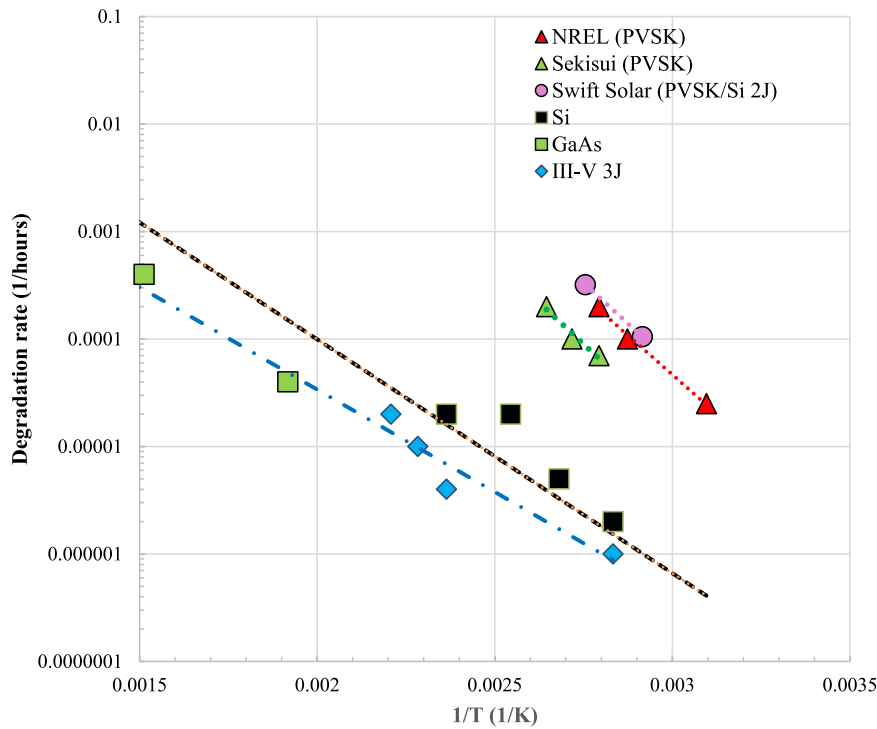


Fig. 10. Arrhenius plots for temperature dependent degradations of perovskite, Perovskite/Si, Si and III-V compound solar cells.

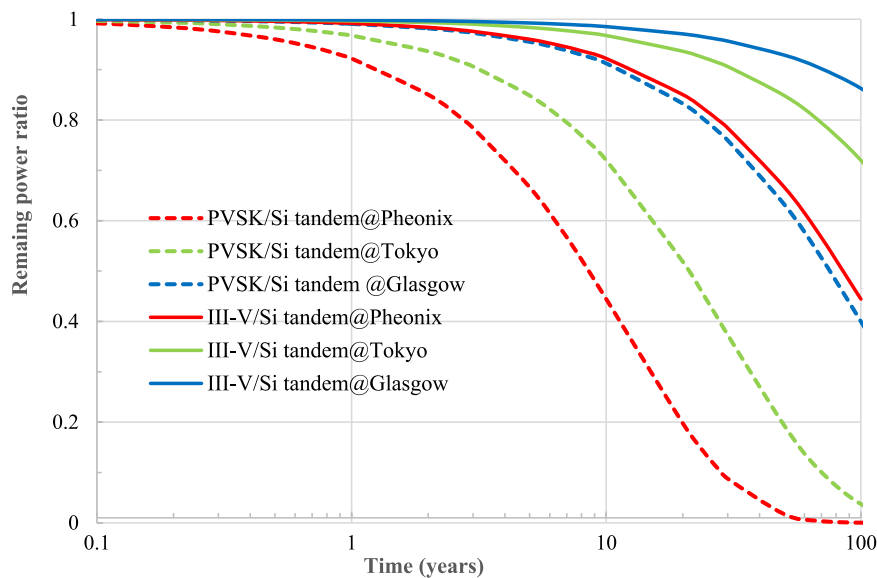


Fig. 11. Analytical results for outdoor degradation of perovskite/Si and III-V/Si tandem solar cells to be operated in Phoenix, Tokyo and Glasgow.

respectively that are shorter with about one order compared to those (27.5 years, 68 years and 150 year) of III-V/Si tandem solar cells.

In addition, light degradation of perovskite-based solar cell modules is another factor affecting performance of perovskite/Si tandem solar cells. In the case of C_{60} -based perovskite solar cells, light illumination degradation rate is estimated to be $2.7 \times 10^{-5} \text{ h}^{-1}$.¹⁴⁹⁾ On the other hands, the III-V solar cells are UV-resistant as demonstrated by space qualification and Si solar cells are UV-resistant because of bottom cell use. Improvement in reliability of perovskite and perovskite/Si tandem solar cells is very important for many applications, although field performance of perovskite and perovskite/Si tandem solar cells tested by SNL and

NREL¹⁵⁰⁾ was improved from average 0.4 years and maximum 0.8 years for perovskite modules and average 0.15 years and maximum 0.35 years for perovskite/Si tandem modules updated in 8 July, 2024 to average 0.75 years and maximum 1.7 years for perovskite modules and average 0.4 years and maximum 1 years for perovskite/Si tandem modules updated in 14 August, 2025.

4. Summary

This paper presented overviews and future perspectives of the Si-based tandem solar cells. The Si-based tandem solar cells have already demonstrated higher efficiency compared to single-junction Si solar cells and have great efficiency potential of more than 39% and 44% for 2-junction and 3-

junction devices, respectively. At present, III–V/Si and perovskites/Si tandem solar cells lead the conversion efficiency tables of Si-based tandem solar cells with demonstrated efficiencies of 36.1% for III–V/Si 3-junction tandem solar cell and 34.85% and 35% for perovskite/Si tandem solar cells, respectively. Additionally, a 33.7%-efficient III–V/Si 3-junction solar cell module with an area of 775 cm² has also been demonstrated, showing an attractiveness for solar-vehicle application. However, Si-based tandems still face an efficiency gap compared to pure III–V 3-junction solar cells with a record efficiency of 39.5%. Thus, further efficiency improvements and cost reduction of the Si tandem solar cells and modules are necessary, if new markets are to be penetrated. As such, perovskite/Si tandem solar cells are expected to be the strongest addition to Si single-junction solar cells as they have shown a great promise in their rapid efficiency development and interest within the Si industry to bring this technology to the market. However, their market penetration will depend not only on their efficiency, but also on their reliable up-scaling and long-term outdoor performance—two aspects that remain critical challenges for the perovskite/Si tandem technology. The development of Si-based tandems with other top-cell materials such as II–VI, chalcogenide, and kesterite is still preliminary and fabricating high-quality materials with tunable bandgaps remains an open question.

Acknowledgments

The authors express sincere thanks to the NEDO and EC for supporting R&D, and to colleagues of Toyota Tech. Inst., FhG-ISE and HZB for their fruitful discussion and cooperation. Toyota Tech. Inst. acknowledges financial support through the NEDO project (Grand Number: 20000938-0). Fraunhofer ISE acknowledges financial support through the BMBF project H2Demo (03SF0619A).

Author Contributions

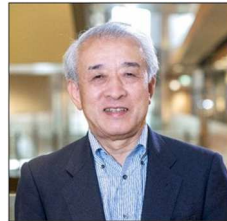
All authors have contributed equally. They have discussed about original plans for this invited review paper and decided their parts. All authors have written their parts, reviewed, discussed, revised and finalized the manuscript.

- 1) Shell, <https://www.shell.com/energy-and-innovation/the-energy-future/scenarios/>.
- 2) N. Haegel et al., *Science* **380**, 39 (2023).
- 3) M. Yamaguchi, Y. Ohshita, H. Shibata, H. Tanpo, and T. Nagai, "Overview and perspective for high-efficiency single-junction solar cells," *Sol. RRL* **7**, 2300308 (2023).
- 4) W. Shockley and H. J. Queisser, "Detailed balance limit of efficiency of p-n junction solar cells," *J. Appl. Phys.* **32**, 510 (1961).
- 5) M. A. Green, E. D. Dunlop, M. Yoshita, N. Kopidakis, K. Bothe, G. Siefert, X. Hao, and J. Y. Jiang, "Solar cell efficiency tables (Version 66)," *Prog. Photovolt.* **33**, 795 (2025).
- 6) M. Yamaguchi, F. Dimroth, N. J. Ekins-Daukes, and Y. Ohshita, "Overview and loss analysis of single-junction and multi-junction solar cells," *EPJ Photovolt.* **13**, 22 (2022).
- 7) A. Goetzberger, J. Luther, and G. Willeke, *Sol. Energy Mater. Sol. Cells* **74**, 1 (2002).
- 8) M. Yamaguchi, F. Dimroth, J. F. Geisz, and N. J. Ekins-Daukes, "Multi-junction solar cells paving the way for super high-efficiency," *J. Appl. Phys.* **129**, 240901 (2021).
- 9) M. Yamaguchi, K.-H. Lee, K. Araki, and N. Kojima, "A review of recent progress in heterogeneous silicon tandem solar cells," *J. Phys. D: Appl. Phys.* **51**, 133002 (2018).
- 10) S. Essig et al., "Raising the one-Sun conversion efficiency of III–V/Si solar cells to 32.8% for two junctions and 35.9% for three junctions," *Nat. Energy* **2**, 17144 (2017).
- 11) P. Schyglulla et al., "Two-terminal III–V/Si triple-junction solar cell with power conversion efficiency of 35.9% at AM1.5g," *Prog. Photovolt.* **30**, 869 (2022).
- 12) A. Al-Ashouri et al., "Monolithic perovskite/silicon tandem solar cell with >29% efficiency by enhanced hole extraction," *Science* **370**, 1300 (2020).
- 13) B. He et al., "Progress in high-efficiency back contacted silicon and perovskite-silicon tandem solar technology at LONG," Presented at the 2025 Global Photovoltaic Conf., Daejeon, Korea, 2025.
- 14) P. Schyglulla et al., "Wafer bonded two-terminal III–V/Si triple-junction solar cell with power conversion efficiency of 36.1% at AM1.5g," *Prog. Photovolt.* **33**, 100 (2025).
- 15) M. Yamaguchi et al., "Development of high-efficiency and low-cost solar cells for PV-powered vehicles application," *Prog. Photovolt.* **29**, 684 (2021).
- 16) P. Schyglulla et al., "Two-terminal III–V/Si triple-junction solar cell with power conversion efficiency of 35.9% at AM1.5g," *Prog. Photovolt.* **30**, 869 (2022).
- 17) G. Létay and A. W. Bett, "EtaOpt—a program for calculating limiting efficiency and optimum bandgap structure for multi-bandgap solar cells and TPV cells," *Proc. 17th European Photovoltaic Solar Energy Conf. and Exhibition (WIP, Munich, 2001)* p. 178.
- 18) I. Vurgaftman, J. R. Meyer, and L. R. Ram-Mohan, "Band parameters for III–V compound semiconductors and their alloys," *J. Appl. Phys.* **89**, 5815 (2001).
- 19) M. Umeno, H. Shimizu, T. Egawa, T. Soga, and T. Jimbo, "GaAs/Si monolithic 2-terminal tandem solar cell grown by MOCVD," 10th European Photovoltaic Solar Energy Conf., 1991 (Lisbon, Portugal) p. 1418.
- 20) T. Soga, T. Kato, M. Yang, and M. Umeno, "High efficiency AlGaAs/Si monolithic tandem solar cell grown by metalorganic chemical vapor deposition," *J. Appl. Phys.* **78**, 4196 (1995).
- 21) R. M. France, F. Dimroth, T. J. Grassman, and R. R. King, "Metamorphic epitaxy for multijunction solar cells," *MRS Bull.* **41**, 202 (2016).
- 22) T. J. Grassman, M. R. Brenner, M. Gonzalez, A. M. Carlin, R. R. Unocic, R. R. Dehoff, M. J. Mills, and S. A. Ringel, "Characterization of metamorphic GaAsP/Si materials and devices for photovoltaic applications," *IEEE Trans. Electron Devices* **57**, 3361 (2010).
- 23) M. Yamaguchi and C. Amano, "Efficiency calculations of thin-film GaAs solar cells on Si substrates," *J. Appl. Phys.* **58**, 3601 (1985).
- 24) K. N. Young, S. Kirmstötter, J. Faucher, A. Gerger, A. Lochtefeld, A. Barnett, and M. L. Lee, "Threading dislocation density characterization in III–V photovoltaic materials by electron channeling contrast imaging," *J. Cryst. Growth* **453**, 65 (2016).
- 25) S. Fan, R. D. Hool, P. Dhingra, M. Kim, E. D. Ratta, B. D. Li, Y. Sun, Z. J. Yu, Z. C. Holman, and M. L. Lee, "Effects of graded buffer design and active region structure on GaAsP single-junction solar cells grown on GaP/Si templates," *Proc. 47th IEEE Photovoltaic Specialists Conf.*, 2020 (Calgary, Canada) p. 2044.
- 26) R. M. France, M. Feifel, J. Belz, A. Beyer, K. Volz, J. Ohlmann, D. Lackner, and F. Dimroth, "Single- and dual-variant atomic ordering in GaAsP compositionally graded buffers on GaP and Si substrates," *J. Cryst. Growth* **506**, 61 (2019).
- 27) I. George, F. Becagli, H. Y. Liu, J. Wu, M. Tang, and R. Beanland, "Dislocation filters in GaAs on Si," *Semicond. Sci. Technol.* **30**, 114004 (2015).
- 28) B. Wang, G. J. Syaranamual, K. H. Lee, S. Bao, Y. Wang, K. E. K. Lee, E. A. Fitzgerald, S. J. Pennycook, S. Gradecak, and J. Michel, "Effectiveness of InGaAs/GaAs superlattice dislocation filter layers epitaxially grown on 200 mm Si wafers with and without Ge buffers," *Semicond. Sci. Technol.* **35**, 95036 (2020).
- 29) M. Feifel et al., "Direct growth of GaInP/GaAs/Si triple-junction solar cell with 22.3% AM1.5g efficiency," *Sol. RRL* **3**, 1900313 (2021).
- 30) J. A. Carlin, C. Andre, O. Kwon, M. Gonzalez, M. Lueck, E. Fitzgerald, D. Wilt, and S. Ringel, "III–V device integration on silicon via metamorphic SiGe substrates," *ECS Trans.* **3**, 729 (2006).
- 31) I. Németh, B. Kunert, W. Stolz, and K. Volz, "Heteroepitaxy of GaP on Si: correlation of morphology, anti-phase-domain structure and MOVPE growth conditions," *J. Cryst. Growth* **310**, 1595 (2008).
- 32) E. L. Warren, A. E. Kibbler, R. M. France, A. G. Norman, P. Stradins, and W. E. McMahon, "Growth of antiphase-domain-free GaP on Si substrates by metalorganic chemical vapor deposition using an in situ AsH₃ surface preparation," *Appl. Phys. Lett.* **107**, 082109 (2015).

- 33) T. E. Saenz, J. S. Mangum, O. D. Schneble, I. Garcia, R. M. France, W. E. McMahon, J. D. Zimmerman, and E. L. Warren, "Towards a III-V solar cell with a metamorphic graded buffer directly grown on v-groove Si substrates," Proc. 48th IEEE Photovoltaic Specialists Conf., 2021p. 1921.
- 34) J. T. Boyer, A. N. Blumer, Z. H. Blumer, D. L. Lepkowski, and T. J. Grassman, "Reduced dislocation introduction in III-V/Si heterostructures with glide-enhancing compressively strained superlattices," *Crystr. Growth Des.* **20**, 6939 (2020).
- 35) T. J. Grassman, D. J. Chmielewski, S. D. Carnevale, J. A. Carlin, and S. A. Ringel, "GaAs_{0.75}P_{0.25}/Si dual-junction solar cells grown by MBE and MOCVD," *IEEE J. Photovolt.* **6**, 326 (2016).
- 36) M. Feifel, D. Lackner, J. Schön, J. Ohlmann, J. Benick, G. Siefer, F. Predan, M. Hermle, and F. Dimroth, "Epitaxial GaInP/GaAs/Si triple-junction solar cell with 25.9% AM1.5g efficiency enabled by transparent metamorphic Al_xGa_{1-x}As_yP_{1-y} step-graded buffer structures," *Sol. RRL* **5**, 2000763 (2021).
- 37) A. Strömberg, B. Manavaimaran, L. Srinivasan, S. Lourduos, and Y.-T. Sun, "Epitaxial lateral overgrowth of GaAsP for III-V/Si-Based photovoltaics," *Phys. Status Solidi A* **220**, 2200623 (2023).
- 38) T. Orzali, A. Vert, B. O'Brien, J. L. Herman, S. Vivekanand, R. J. W. Hill, Z. Karim, and S. S. Papa Rao, "GaAs on Si epitaxy by aspect ratio trapping: Analysis and reduction of defects propagating along the trench direction," *J. Appl. Phys.* **118**, 105307 (2015).
- 39) B. Piccione, C. H. Cho, L. K. van Vugt, and R. Agarwal, "All-optical active switching in individual semiconductor nanowires," *Nat. Nanotechnol.* **7**, 640 (2012).
- 40) J. E. Ayers, L. J. Schowalter, and S. K. Ghandi, "Post-growth thermal annealing of GaAs on Si(001) grown by organometallic vapor phase epitaxy," *J. Cryst. Growth* **125**, 329 (1992).
- 41) S. Essig and F. Dimroth, "Fast atom beam activated wafer bonds between n-Si and n-GaAs with low resistance," *ECS J. Solid State Sci. Technol.* **2**, Q178 (2013).
- 42) L. Vauche et al., "Wafer bonding approaches for III-V on Si multi-junction solar cells," Proc. of the 44th IEEE Photovoltaic Specialists Conf., Washington, DC, USA, 2017 p. 249210.1109/PVSC.2017.8366093.
- 43) S. Bao et al., "A review of silicon-based wafer bonding processes, an approach to realize the monolithic integration of Si-CMOS and III-V-on-Si wafers," *J. Semicond.* **42**, 23106 (2021).
- 44) A. C. Tamboli, M. van Hest, M. Steiner, S. Essig, E. E. Perl, A. G. Norman, N. Bosco, and P. Stradins, "III-V/Si wafer bonding using transparent, conductive oxide interlayers," *Appl. Phys. Lett.* **106**, 263904 (2015).
- 45) T. R. Klein, B. G. Lee, M. Schnabel, E. L. Warren, P. Stradins, A. C. Tamboli, and M. F. van Hest, "Transparent conductive adhesives for tandem solar cells," Proc. of the 44th IEEE Photovoltaic Specialists Conf., Washington, DC, USA, 2017 p. 248210.1109/PVSC.2017.8366090.
- 46) M. Schnabel et al., "Three-Terminal III-V/Si tandem solar cells enabled by a transparent conductive adhesive," *Sustainable Energy Fuels* **4**, 549 (2019).
- 47) A. van Geelen, P. R. Hageman, G. J. Bauhuis, P. C. van Rijsingen, P. Schmidt, and L. J. Giling, "Epitaxial lift-off GaAs solar cell from a reusable GaAs substrate," *Mater. Sci. Eng. B* **45**, 162 (1997).
- 48) C.-W. Cheng, K.-T. Shiu, N. Li, S.-J. Han, L. Shi, and D. K. Sadana, "Epitaxial lift-off process for gallium arsenide substrate reuse and flexible electronics," *Nat. Commun.* **4**, 1577 (2013).
- 49) K. Xiong et al., "AlGaAs/Si dual-junction tandem solar cells by epitaxial lift-off and print-transfer-assisted direct bonding," *Energy Sci. Eng.* **6**, 47 (2018).
- 50) B. Bläsi et al., "Photonic structures for III-V//Si multijunction solar cells with efficiency >33%," Proc. of the Photonics for Solar Energy Systems VII, Strasbourg, France, 2018 p. 210.1117/12.2307831..
- 51) A. Cordaro, R. Müller, S. W. Tabernig, N. Tucher, P. Schygulla, O. Höhn, B. Bläsi, and A. Polman, "Nanopatterned back-reflector with engineered near-field/far-field light scattering for enhanced light trapping in silicon-based multijunction solar cells," *ACS Photonics* **10**, 4061 (2023).
- 52) U. Heitmann, J. Bartsch, S. Kluska, H. Hauser, O. Höhn, R. Hermann, D. Lackner, S. Janz, and S. W. Glunz, "Pathways and potentials for III-V on Si tandem solar cells realized using a ZnO-Based transparent conductive adhesive," *IEEE J. Photovolt.* **11**, 85 (2021).
- 53) U. Heitmann, O. Höhn, H. Hauser, S. Kluska, J. Bartsch, and S. Janz, "Electrical and optical analysis of a spray coated transparent conductive adhesive for two-terminal silicon based tandem solar cells," *AIP Conf. Proc.* **2147**, 130001 (2019).
- 54) K. Makita et al., "III-V/Si multijunction solar cells with 30% efficiency using smart stack technology with Pd nanoparticle array," *Prog. Photovolt. Res. Appl.* **42** (2019).
- 55) K. T. VanSant, A. C. Tamboli, and E. L. Warren, "III-V-on-Si tandem solar cells," *Joule* **5**, 514 (2021).
- 56) O. Höhn, M. Hanser, M. Steiner, E. Lorenz, B. Bläsi, S. W. Glunz, and F. Dimroth, "Energy yield and performance ratio of III-V on silicon dual junction solar cells in different climate zones," Proc. of the 38th European Photovoltaic Solar Energy Conf.online, 2021 p. 51510.4229/EUPVSEC20212021-3BV.2.66.
- 57) H. Schulte-Huxel, D. J. Friedman, and A. C. Tamboli, "String-level modeling of two, three, and four terminal Si-Based tandem modules," *IEEE J. Photovolt.* **8**, 1370 (2018).
- 58) M. Yamaguchi, T. Takamoto, H. Juso, K. Nakamura, R. Ozaki, T. Masuda, T. Mabuchi, K. Okumura, N. Kojima, and Y. Ohshita, "Approaches for III-V/Si tandem solar cells and comparative studies on Si tandem solar cells," *Prog. Photovolt.* **33**, 116 (2025).
- 59) A. Kojima, K. Teshima, Y. Shirai, and T. Miyasaka, "Organometal halide perovskites as visible-light sensitizers for photovoltaic cells," *J. Am. Chem. Soc.* **131**, 6050 (2009).
- 60) "Best research-cell efficiency chart Accessed: Dec. 15, 2025. [Online]. Available: <https://nrel.gov/pv/cell-efficiency.html>.
- 61) E. L. Unger, L. Kegelmann, K. Suchan, D. Sörell, L. Korte, and S. Albrecht, "Roadmap and roadblocks for the band gap tunability of metal halide perovskites," *J. Mater. Chem. A* **5**, 11401 (2017).
- 62) J. H. Noh, S. H. Im, J. H. Heo, T. N. Mandal, and S. I. Seok, "Chemical management for colorful, efficient, and stable inorganic-organic hybrid nanostructured solar cells," *Nano Lett.* **13**, 1764 (2013).
- 63) K. A. Bush et al., "Compositional engineering for efficient wide band gap perovskites with improved stability to photoinduced phase segregation," *ACS Energy Lett.* **3**, 428 (2018).
- 64) M. Saliba et al., "Cesium-containing triple cation perovskite solar cells: improved stability, reproducibility and high efficiency," *Energy Environ. Sci.* **9**, 1989 (2016).
- 65) D. W. deQuilettes et al., "Photoluminescence lifetimes exceeding 8 μs and quantum yields exceeding 30% in hybrid perovskite thin films by ligand passivation," *ACS Energy Lett.* **1**, 438 (2016).
- 66) M. Stolterfoht et al., "Visualization and suppression of interfacial recombination for high-efficiency large-area pin perovskite solar cells," *Nat. Energy* **3**, 847 (2018).
- 67) S. D. Stranks et al., "Electron-hole diffusion lengths exceeding 1 micrometer in an organometal trihalide perovskite absorber," *Science* **342**, 341 (2013).
- 68) B. Roose, Q. Wang, and A. Abate, "The role of charge selective contacts in perovskite solar cell stability," *Adv. Energy Mater.* **9**, 1803140 (2019).
- 69) Y. Wang et al., "PTAA as efficient hole transport materials in perovskite solar cells: a review," *Sol. RRL* **6**, 2200234 (2022).
- 70) A. Al-Ashouri et al., "Conformal monolayer contacts with lossless interfaces for perovskite single junction and monolithic tandem solar cells," *Energy Environ. Sci.* **12**, 3356 (2019).
- 71) L. Nakka, Y. Cheng, A. G. Aberle, and F. Lin, "Analytical review of Spiro-OMeTAD hole transport materials: paths toward stable and efficient perovskite solar cells," *Adv. Energy Sustain. Res.* **3**, 2200045 (2022).
- 72) L. Duan et al., "Stability challenges for the commercialization of perovskite-silicon tandem solar cells," *Nat. Rev. Mater.* **8**, 261 (2023).
- 73) H. Zhu et al., "Long-term operating stability in perovskite photovoltaics," *Nat. Rev. Mater.* **8**, 569 (2023).
- 74) I. Celik et al., "Environmental analysis of perovskites and other relevant solar cell technologies in a tandem configuration," *Energy Environ. Sci.* **10**, 1874 (2017).
- 75) N. Bartie et al., "Cost versus environment? Combined life cycle, techno-economic, and circularity assessment of silicon- and perovskite-based photovoltaic systems," *J. Ind. Ecol.* **27**, 993 (2023).
- 76) C. Messmer et al., "The race for the best silicon bottom cell: efficiency and cost evaluation of perovskite-silicon tandem solar cells," *Prog. Photovolt. Res. Appl.* **29**, 744 (2021).
- 77) M. Jaysankar et al., "Four-terminal perovskite/silicon multijunction solar modules," *Adv. Energy Mater.* **7**, 1602807 (2017).
- 78) B. Chen et al., "Enhanced optical path and electron diffusion length enable high-efficiency perovskite tandems," *Nat. Commun.* **11**, 1257 (2020).
- 79) D. Yang et al., "28.3%-efficiency perovskite/silicon tandem solar cell by optimal transparent electrode for high efficient semitransparent top cell," *Nano Energy* **84**, 105934 (2021).
- 80) A. Abbasiyan, M. Noori, and H. Baghban, "A highly efficient 4-terminal perovskite/silicon tandem solar cells using QIBC and IBC configurations in the top and bottom cells, respectively," *Mater. Today Energy* **28**, 101055 (2022).
- 81) "Solliance hits 29.2% efficiency on perovskite/silicon tandem solar cell—pv magazine International Accessed: Apr. 17, 2024. [Online]. Available:

- <https://pv-magazine.com/2021/11/01/solliance-hits-29-2-efficiency-on-perovskite-silicon-tandem-solar-cell/>.
- 82) "Imec hits 27.1% on perovskite/silicon tandem cell—pv magazine International. Accessed: Apr. 17, 2024. [Online]. Available: <https://pv-magazine.com/2018/07/24/imec-hits-27-1-on-perovskite-silicon-tandem-cell/>.
 - 83) L. Duan et al., "Stability challenges for the commercialization of perovskite–silicon tandem solar cells," *Nat. Rev. Mater.* **8**, 261 (2023).
 - 84) Continental Energy Solutions, CubicPV - Direct Wafer, Tandem, Perovskite Solar Technology | Frank van Mierlo, CEO | CPH Ep.55, (Aug. 13, 2021). Accessed: Apr. 17, 2024. [Online]. Available: <https://youtube.com/watch?v=1pUVSr2tBZo>.
 - 85) S. Albrecht et al., "Monolithic perovskite/silicon-heterojunction tandem solar cells processed at low temperature," *Energy Environ. Sci.* **9**, 81 (2016).
 - 86) K. A. Bush et al., "23.6%-efficient monolithic perovskite/silicon tandem solar cells with improved stability," *Nat. Energy* **2**, 17009 (2017).
 - 87) F. Sahli et al., "Fully textured monolithic perovskite/silicon tandem solar cells with 25.2% power conversion efficiency," *Nat. Mater.* **17**, 820 (2018).
 - 88) M. Jošt et al., "Textured interfaces in monolithic perovskite/silicon tandem solar cells: advanced light management for improved efficiency and energy yield," *Energy Environ. Sci.* **11**, 3511 (2018).
 - 89) J. Xu et al., "Triple-halide wide-band gap perovskites with suppressed phase segregation for efficient tandems," *Science* **367**, 1097 (2020).
 - 90) X. Y. Chin, "Interface passivation for 31.25%-efficient perovskite/silicon tandem solar cells," *Science* **381**, 50 (2023).
 - 91) S. Mariotti et al., "Interface engineering for high-performance, triple-halide perovskite–silicon tandem solar cells," *Science* **381**, 63 (2023).
 - 92) E. Aydin et al., "Enhanced optoelectronic coupling for perovskite-silicon tandem solar cells," *Nature* **623**, 732 (2023).
 - 93) Y. Hou et al., "Efficient tandem solar cells with solution-processed perovskite on textured crystalline silicon," *Science* **367**, 1135 (2020).
 - 94) "33.5% - LONGi announces new conversion efficiency for its silicon-perovskite tandem solar cells at Intersolar Europe 2023. Accessed: Apr. 17, 2024. [Online]. Available: <https://longi.com/en/distributorbriefing/longi-reached-new-record/undefined/>.
 - 95) "Oxford PV and fraunhofer ISE develop full-sized tandem PV module with record efficiency of 25 percent - fraunhofer ISE. Accessed: Apr. 17, 2024. [Online]. Available: <https://ise.fraunhofer.de/en/press-media/press-releases/2024/oxford-pv-and-fraunhofer-ise-develop-full-sized-tandem-pv-module-with-record-efficiency-of-25-percent.html>.
 - 96) "Qcells and Helmholtz-Zentrum Berlin achieve record efficiency of 28.7% for 2-terminal perovskite-silicon tandem solar cell. Accessed: Apr. 17, 2024. [Online]. Available: https://q-cells.eu/it/press-releases/detail?tx_news_pi1%5Baction%5D=detail&tx_news_pi1%5Bcontroller%5D=News&tx_news_pi1%5Bnews%5D=8&cHash=86164f7f82bb61afae35b4d6e470721f.
 - 97) K. Sveinbjörnsson et al., "Monolithic perovskite/silicon tandem solar cell with 28.7% efficiency using industrial silicon bottom cells," *ACS Energy Lett.* **7**, 2654 (2022).
 - 98) Jedics, "Meyer Burger to commercialize 29.6%-efficient perovskite tandem solar cells. Accessed: Apr. 17, 2024. [Online]. Available: <https://pv-magazine.com/2022/12/14/meyer-burger-to-commercialize-29-6-efficient-perovskite-tandem-solar-cells/>.
 - 99) M. Carmody, S. Mallick, J. Margetis, R. Kodama, T. Biegala, D. Xu, P. Bechmann, J. W. Garland, and S. Sivananthan, "Single-crystal II-VI on Si single-junction and tandem solar cells," *Appl. Phys. Lett.* **96**, 153502 (2010).
 - 100) F. Martinho et al., "Nitride-based interfacial layers for monolithic tandem integration of new solar energy materials on Si: the case of CZTS," *ACS Appl. Energy Mater.* **3**, 4600 (2020).
 - 101) J. Kwon et al., "Two-terminal DSSC/silicon tandem solar cells exceeding 18% efficiency," *Energy Environ. Sci.* **9**, 3657 (2016).
 - 102) H. Park, S. H. Park, S.-W. Lee, Y. Kang, D. Kim, H. J. Son, and H.-S. Lee, "Novel polymer-based organic/c-Si monolithic tandem solar cell: enhanced efficiency using interlayer and transport top electrode engineering," *Macromol. Rapid Commun.* **42**, 2100305 (2021).
 - 103) N. Nakagawa, S. Shibusaki, Y. Honishi, M. Yamazaki, Y. Hiraoka, and K. Yamamoto, "Development of a Zn-based n-layer in cuprous oxide top cells for high-efficiency tandem photovoltaics," Proc. of the 47th IEEE Photovoltaic Specialists Conf. (IEEE, New York, 2020 p. 98310.1109/PVSC45281.2020.9300600).
 - 104) M. Kanematsu, R. Mishima, H. Uzu, D. Adachi, and K. Yamamoto, "High efficiency perovskite single junction solar module and its application to tandem solar cell," Presented at the 34th Int. Photovoltaic Science and Technology Conf., Shenzhen, China, 2023.
 - 105) R. Lang, J. Schon, F. Dimroth, and D. Lackner, "Optimization of GaAs solar cell performance and growth efficiency at MOVPE growth rates of 100 $\mu\text{m}/\text{h}$," *IEEE J. Photovolt.* **1**, 1596 (2018).
 - 106) R. Lang, F. Habib, M. Dauelsberg, F. Dimroth, and D. Lackner, "MOVPE growth of GaAs with growth rates up to 280 $\mu\text{m}/\text{h}$," *J. Cryst. Growth* **537**, 125601 (2020).
 - 107) W. Metaferia, K. L. Schulte, J. Simon, S. Johnston, and A. J. Ptak, "Gallium arsenide solar cells grown at rates exceeding 300 $\mu\text{m h}^{-1}$ by hydride vapor phase epitaxy," *Nat. Commun.* **10**, 3361 (2019).
 - 108) J. W. Boucher, A. L. Greenaway, A. J. Ritenour, A. L. Davis, B. F. Bachman, S. Aloni, and S. W. Boettcher, "Low-cost growth of III-V layers on Si using close-spaced vapor transport," Proc. of the 42nd IEEE Photovoltaic Specialist Conf., New Orleans, USA, 2015 p. 110.1109/PVSC.2015.7356079.
 - 109) K. T. VanSant et al., "Toward low-cost 4-Terminal GaAs/Si Tandem solar cells," *ACS Appl. Energy Mater.* **2**, 2375 (2019).
 - 110) J. Schube et al., "Mask and plate: a scalable front metallization with low-cost potential for III-V-based tandem solar cells enabling 31.6% conversion efficiency," *Sci. Rep.* **13**, 15745 (2023).
 - 111) N. Hayati-Roodbari, A. Wheeldon, A. Fian, and R. Trattning, "1,8-Octanedithiol as an effective intermediate layer for deposition of Cu electrodes via inkjet printing and laser sintering on III-V triple-junction solar cells," *Phys. Status Solidi A* **219**, 2200089 (2022).
 - 112) J. D. Wood, C. L. Stender, C. T. Youtsey, D. Rowell, A. Wibowo, M. Osowski, and N. Pan, "Screen Printed Contacts to III-V epilayers for low cost photovoltaics," Proc. of the 7th World Conf. on Photovoltaic Energy Conversion: Joint Conf. of 34th European Photovoltaic Solar Energy Conf. and Exhibition, 45th US IEEE Photovoltaic Specialists Conf., 28th Asia/Pacific PV Science and Engineering Conf., Waikoloa, Hawaii, USA, 2018 p. 385310.1109/PVSC.2018.8547701.
 - 113) Shygyulla, "Patrick. III-V-semiconductor subcell absorbers in silicon-based triple-junction solar cells," Dissertation Universität Freiburg 10.6094/UNIFR/233991 (2023).
 - 114) R. Müller et al., "Silicon-based monolithic triple-junction solar cells with conversion efficiency >34%," Proc. of the 37th European Photovoltaic Solar Energy Conf. and Exhibition, Lisbon, Portugal, 2020 p. 57410.4229/EUPVSEC20202020-3AO.7.2..
 - 115) C. F. Blanco, S. Cucurachi, F. Dimroth, J. B. Guinée, W. J. G. M. Peijnenburg, and M. G. Vijver, "Environmental impacts of III-V/silicon photovoltaics: life cycle assessment and guidance for sustainable manufacturing," *Energy Environ. Sci.* **13**, 4280 (2020).
 - 116) C. F. Blanco, J. T. K. Quik, M. Hof, A. Fuortes, P. Behrens, S. Cucurachi, W. J. G. M. Peijnenburg, F. Dimroth, and M. G. Vijver, "A prospective ecological risk assessment of high-efficiency III-V/silicon tandem solar cells," *Environ. Sci. Process. Impacts* **26**, 540 (2024).
 - 117) C. C. Boyd et al., "Overcoming redox reactions at perovskite-nickel oxide interfaces to boost voltages in perovskite solar cells," *Joule* **4**, 1759 (2020).
 - 118) M. V. Khenkin et al., "Consensus statement for stability assessment and reporting for perovskite photovoltaics based on ISOS procedures," *Nat. Energy* **5**, 35 (2020).
 - 119) Q. Emery et al., "Encapsulation and outdoor testing of perovskite solar cells: comparing industrially relevant process with a simplified lab procedure," *ACS Appl. Mater. Interfaces* **14**, 5159 (2022).
 - 120) J. Liu et al., "28.2%-efficient, outdoor-stable perovskite/silicon tandem solar cell," *Joule* **5**, 3169 (2021).
 - 121) M. De Bastiani et al., "Toward stable monolithic perovskite/silicon tandem photovoltaics: a six-month outdoor performance study in a hot and humid climate," *ACS Energy Lett.* **6**, 2944 (2021).
 - 122) D. H. Kim, J. B. Whitaker, Z. Li, M. F. A. M. van Hest, and K. Zhu, "Outlook and challenges of perovskite solar cells toward terawatt-scale photovoltaic module technology," *Joule* **2**, 1437 (2018).
 - 123) H. Eggers et al., "Inkjet-printed micrometer-thick perovskite solar cells with large columnar grains," *Adv. Energy Mater.* **10**, 1903184 (2020).
 - 124) 'Japan's NEDO and Panasonic Achieve the World's Highest Conversion Efficiency of 16.09% for Largest-area Perovskite Solar Cell Module | Innovations/Technologies | Company | Press Release,' Panasonic Newsroom Global. Accessed: Apr. 17, 2024. [Online]. Available: <https://news.panasonic.com/global/press/en/200207-2>.
 - 125) S. K. Podapangi et al., "Green solvents, materials, and lead-free semiconductors for sustainable fabrication of perovskite solar cells," *RSC Adv.* **13**, 18165 (2023).
 - 126) A. E. Magdalin et al., "Development of lead-free perovskite solar cells: Opportunities, challenges, and future technologies," *Results Eng.* **20**, 101438 (2023).

- 127) H. Zhang et al., "Lead immobilization for environmentally sustainable perovskite solar cells," *Nature* **617** (2023).
- 128) P. Wu et al., "Beyond efficiency fever: preventing lead leakage for perovskite solar cells," *Matter* **5**, 1137 (2022).
- 129) U. Rau, "Reciprocity relation between photovoltaic quantum efficiency and electroluminescent emission of solar cells," *Phys. Rev.* **B76**, 085303 (2007).
- 130) J. Yao et al., "Quantifying losses in open-circuit voltage in solution-processable solar cells," *J. Phys. Rev. Appl.* **4**, 014020 (2015).
- 131) M. Yamaguchi, H. Yamada, Y. Katsumata, K.-H. Lee, K. Araki, and N. Kojima, "Efficiency potential and recent activities of high-efficiency solar cells," *J. Mater. Res.* **32**, 3446 (2017).
- 132) M. Yamaguchi, K. H. Lee, K. Araki, N. Kojima, H. Yamada, and Y. Katsumata, "Analysis for efficiency potential of high-efficiency and next generation solar cells," *Prog. Photovolt.* **26**, 543 (2018).
- 133) M. Yamaguchi, K.-H. Lee, P. Schyulla, F. Dimroth, T. Takamoto, R. Ozaki, K. Nakamura, N. Kojima, and Y. Ohshita, "Approaches for high-efficiency III-V/Si tandem solar cells," *Energy Power Eng.* **13**, 413 (2021).
- 134) M. A. Green, *Solar Cells* (UNSW, Kensington, 1998) p. 96.
- 135) R. M. Kayes, H. Nie, R. Twist, S. G. Spruytte, F. Reinhardt, I. Kizilyalli, and G. Higashi, "27.6 conversion efficiency, a new record for single-junction solar cells under 1 Sun illumination," Proc. of the 37th IEEE Photovoltaic Specialists Conf. (IEEE, New York., 2011 p. 410.1109/PVSC.2011.6185831.
- 136) T. J. Macdonald, L. Lanzetta, X. Liang, D. Ding, and S. A. Haque, "Engineering stable lead-free tin halide perovskite solar cells: lessons from materials chemistry," *Adv. Mater.* **35**, 2206684 (2023).
- 137) S. E. Sofia, H. Wang, A. Bruno, J. L. Cruz-Campa, T. Buonassisi, and I. M. Peters, "Roadmap for cost-effective, commercially-viable perovskite silicon tandem for the current and future PV market," *Sustainable Energy Fuels* **4**, 852 (2020).
- 138) VDMA, International Technology Roadmap for Photovoltaics (ITRPV) 14th ed. (2023) itrpv.org.pv.vdma.org.
- 139) V. Benda and L. Cerna, "A note on limits and trends in PV cells and modules," *Appl. Sci.* **12**, 3363 (2022).
- 140) N. Rolston, W. J. Scheideler, A. C. Flick, J. P. Chen, H. Elmaraghi, A. Sleugh, O. Zhao, M. Woodhouse, and R. H. Dauskardt, "Rapid open-air fabrication of perovskite solar modules," *Joule* **4**, 2675 (2020).
- 141) Q. Jiang and K. Zhu, "Rapid advances enabling high-performance inverted perovskite solar cells," *Nat. Rev. Mater.* **9**, 399 (2024).
- 142) A. Mavlonov, Y. Hishikawa, Y. Kawano, T. Negami, A. Hayakawa, S. Tsujimura, T. Okumura, and T. Minemoto, "Thermal stability test on flexible perovskite solar cell modules to estimate activation energy of degradation on temperature," *Sol. Energy Mater. Sol. Cells.* **277**, 113148 (2024).
- 143) J. Jean, Tandems and more at TW4 presented at the 4th Terawatt Workshop, 2024.
- 144) M. Winter, D. C. Walter, B. Min, R. Peibst, R. Brendel, and J. Schmidt, "Light and elevated temperature induced degradation and recovery of gallium-doped Czochralski-silicon solar cells," *Sci. Rep.* **16**, 8089 (2022).
- 145) S. Matsuda, M. Otsuda, K. Mitsui, M. Kato, S. Hokuo, and S. Yoshida, "Manufacturing status of GaAs solar cells for space applications," Proc. of the 17th IEEE Photovoltaic Specialists Conf. (IEEE, New York., 1984 p. 97.
- 146) M. Yamaguchi, T. Takamoto, K. Araki, and N. Kojima, "Recent progress for concentrator photovoltaics in Japan," *Jpn. J. Appl. Phys.* **55**, 04EA05 (2016).
- 147) M. Yamaguchi et al., "Analysis for effects of temperature rise of PV modules upon driving distance of vehicle integrated photovoltaic electric vehicles," *Energy Power Eng.* **16**, 131 (2024).
- 148) Weatherspark, <https://ja.weatherspark.com/>.
- 149) C. Zhao et al., "Stabilization of highly efficient perovskite solar cells with a tailored supramolecular interface," *Nat. Commun.* **15**, 7139 (2024).
- 150) SNL and NREL, PVPACT. <https://pvpact.sandia.gov/results-and-data/>.



Masafumi Yamaguchi has received his Ph.D. degree from Hokkaido University, Japan (1978). He is now Professor Emeritus and Invited Research Fellow at the Toyota Technological Institute, Japan, Visiting Professor, Chiba Institute of Technology, Chairman of the PV Project Review Committee under the NEDO. He has received numerous awards such as the Becquerel Prize from the European Commission in 2004, the William Cherry Award from the IEEE in 2008, the PVSEC Award in 2011, the WCPEC Award in

2014 and the Purple Ribbon Medal from the Emperor in 2025 for his outstanding contribution to the development of science and technology of photovoltaic solar energy, and to the International collaboration and cooperation.



Patrick Schyulla studied physics at the Imperial College London and the Ruprecht-Karls University in Heidelberg where he obtained his Bachelor's and Master's degrees. In 2018 he moved to Freiburg and started working at the Fraunhofer Institute for Solar Energy Systems ISE on III-V-on-silicon triple-junction solar cells. He received a Ph.D. by the Technical Faculty of the University of Freiburg in 2023 and continued to work as a postdoc focusing on epitaxy and optical simulations of high-efficiency III-V solar cells and photonic power converters.



Frank Dimroth has been working on III-V tandem photovoltaics since the late 1990s. Today he is co-heading the department "III-V photovoltaics and concentrator technology" at Fraunhofer ISE in Freiburg, Germany where his team performs applied research on next generation III-V technologies including CPV, space solar cells, laser power converters and thermophotovoltaics. Numerous record efficiencies for PV cells and modules as well as ~400 scientific publications have been the outcome of this work.